Research Square

Preprints are preliminary reports that have not undergone peer review.
They should not be considered conclusive, used to inform clinical practice,
or referenced by the media as validated information.

Schrödinger's Continuous Electron Revisited: A Fourth Spatial Direction Recovers Exchange, Exclusion and the Born Rule Without Configuration Space

Dinesh Vidhani

dvidhani@mdc.edu

Miami Dade College https://orcid.org/0000-0001-6846-1557

Research Article

Keywords: Continuous electronic matter, Schrödinger charge density, Configuration space, Fourth spatial dimension, Exchange antisymmetry, Pauli exclusion principle, Born rule, Atomic structure

Posted Date: November 27th, 2026

DOI: https://doi.org/10.21203/rs.3.rs-11884360/v1

License: This work is licensed under a Creative Commons Attribution 4.0 International License.
Read Full License

Additional Declarations: The authors declare no competing interests.

Schrödinger's Continuous Electron Revisited: A Fourth Spatial Direction Recovers Exchange, Exclusion and the Born Rule Without Configuration Space

Dinesh V. Vidhani,*[1,2]

[1]Department of Chemistry & Biochemistry, Florida State University, 95 Chieftain Way, Tallahassee, FL, 33134.
[2]Department of Math & Natural Science, Miami Dade College, 627 SW 27th Ave, Miami, FL, 33135, USA.
Author Contact E-mail: dvidhani@mdc.edu

ABSTRACT

In 1926, Schrödinger interpreted his wave as a real, continuous distribution of electronic matter. This interpretation was soon challenged for four reasons: the many-electron wave exists in configuration space, electrons are detected as whole entities, a charged cloud would be expected to repel itself, and classical charged matter cannot possess spin or exhibit magnetism. The objective of this study is to determine the conditions under which the electron can be treated as a continuous body that addresses these objections and aligns with spectroscopic evidence, as well as to introduce a corresponding physical model of the atom. By conceptualizing the vacuum as an unbounded resonator vibrating at Ω_0, electronic matter as maintaining this resonance, and the nucleus as a compact 1/r source, the vacuum-resonance continuous-matter (VRCM) model provides a physical foundation for the atom. This model further conceptualizes the electron as a continuous body extending into a real fourth spatial direction (w), with a maximum extent of 2.6×10^{-19} m, and whose portions are defined by pattern, fold, and side. A single calibrated action unit, Γ, reproduced fifteen lines of H, He^+, and Li^{2+} within 2.9 ppm, and one value of Γ fitted five measured hydrogen transitions within 1.3×10^{-9}. Unlike non-relativistic quantum mechanics, which postulates the sign reversal upon exchanging two electrons, VRCM derives it from the geometry of its body, which is non-orientable and returns only after 720°. With each place holding one hydrogen-equivalent of matter and a face rule taken as a premise, each pattern accommodates only two portions, one on each side, which accounted for the shells from hydrogen to neon, lithium's 2s below its 2p within 3%, the ground terms from boron to fluorine through Hund's first two rules, and the triplet ground state of O_2. The diamagnetism of helium and the paramagnetic susceptibility of O_2 agreed

within 0.7% and 0.5%, respectively, and the ionization energy of lithium came out at 5.409 eV against the measured 5.392 eV. Helium's two portions share one three-dimensional region and are separated only along w; without w, its energy rises by at least 20 eV. A coupling of the vibrations of the two portions through w, fixed on helium alone, brought the correlation energies of the helium-like ions from Li^{+} to Ne^{+8} within 0.1% and of H^{-} within 1.6%. Within one side, the self-repulsion of the body is cancelled exactly by exchange, while portions on opposite sides repel with full strength. With the coupling between the two faces taken as a premise, a two-face law gave $g = 2$, the two kinds of charge as the two faces, and Dirac's small component as matter spilled onto the second face. The vacuum's zero-point vibrations gave the Lamb shift of hydrogen as 1050.74 MHz at one loop, against the measured 1057.8 MHz, and the electron's anomalous magnetic moment as $\alpha/2\pi$. Aside from spectra, the same body accounted for its detection as a whole: its wavelength followed from the vacuum's wave rule, and the Born odds from the body remaining whole as it contracts onto one place at capture, given a detection threshold taken as a premise. Each premise in this model was adopted only after its alternative failed by a stated margin. These results suggest that continuous electronic matter connected through the fourth spatial direction (*w*) can recover the exchange sign, exclusion and the Born rule without configuration space, while accounting for spin, magnetism and the absence of self-repulsion.

INTRODUCTION

Quantum mechanics offers a highly precise account of atomic and molecular structures. Nevertheless, the ontological status of the electronic wave function, especially whether it represents a physically extended distribution or encodes probabilities for measurement outcomes, remains a subject of foundational debate. In 1926, Schrödinger proposed that the wave function represents a real distribution of electronic charge, continuously distributed throughout space with a density proportional to the squared amplitude.[1,2] This interpretation was appealing because it provided a visualizable model of the atom in which each stationary state has a characteristic spatial structure. This interpretation faces four principal objections that continue to challenge any continuous-matter model. First, the conventional wave function for many electrons is defined in terms of 3N spatial coordinates, whereas physical matter is observed in 3D physical space only. While a three-dimensional electron density can be derived from the many-electron wave function, such treatment generally tends to lose information about electron-electron correlations.[3] Second, detectors observe electrons as discrete entities at specific locations rather than spatially distributed fractional charge. Born's statistical interpretation of scattering

processes provided an alternative understanding of the wave function, later developed into the familiar position-probability rule.[4] Third, interpreting the electronic density as an ordinary classical charge distribution introduces electrostatic self-interaction. However, in exact quantum treatments, this spurious one-electron self-interaction is canceled and does not contribute to observable energies. Hence, a continuous electronic-matter model should be able to explain how self-interaction is avoided or consistently incorporated without compromising atomic spectra.[2,5] Fourth, conventional classical statistical mechanics predicts no equilibrium orbital magnetism, as expressed by the Bohr–van Leeuwen theorem. A continuous-electronic-matter model must therefore explain intrinsic electron magnetic moments and their observed response to magnetic fields.[6,7] Finally, a simple classical model that identifies electron spin with rigid rotation of a charged mass distribution faces serious difficulties, including superluminal surface velocities and a gyromagnetic factor of g=1 rather than the observed value near 2. These objections do not necessarily apply to relativistic field descriptions, in which spin and magnetic moment may arise from more general energy and charge currents.[8,9,10,11,12]

Nonetheless, the idea of a physical description of electronic matter and wave dynamics has persisted. For example, Madelung reformulated Schrödinger's equation in the form of hydrodynamics, analogous to the flow of a fluid, but full equivalence with quantum mechanics requires an additional quantization condition.[13,14] In contrast de Broglie's pilot-wave ideas and Bohm's subsequent hidden-variable formulation instead retain particle positions as the material ontology, with the wave function governing their motion.[15,16] Furthermore, semiclassical radiation theories have examined the interaction of quantum matter with classical electromagnetic fields, while self-field formulations have investigated radiative phenomena using a classical radiation field coupled to electronic dynamics.[17,18] Within relativistic wave-field theory, Ohanian interpreted spin and magnetic moment through circulating energy and charge currents. A further ontological development is provided by the mass-density formulation of spontaneous-collapse theories, particularly GRWm, which assigns a real matter density to ordinary three-dimensional space while retaining a many-body wave function and modified stochastic quantum dynamics.[19,20,21] However, such models also introduce testable departures from standard quantum dynamics and are constrained by experimental bounds on spontaneous radiation, excess heating, and related effects.[22]

While these approaches address different aspects of quantum dynamics and ontology, an independently formulated theory of continuous electronic matter that avoids configuration-space ontology has not yet been developed. Any such description must explain discrete atomic spectra, localized detection, electromagnetic interactions, spin, and fermionic behavior. Its predictive power therefore requires quantitative comparison

with established quantum-mechanical results and spectroscopic observations. This study develops a candidate Vacuum-Resonance Continuous-Matter (VRCM) model by systematically evaluating alternative approaches.

The contributions of the present work are threefold. First, it introduces a continuous-matter description that addresses the major historical objections to Schrödinger's original model by implementing rules validated through quantitative experimental tests. Within this framework, the model reproduces fifteen one-electron lines of H, He^{+} and Li^{+2} within 2.9 ppm, the hydrogen Lamb shift to within 0.7% at one loop with no imported constant, and the correlation, ionization, diamagnetic and paramagnetic properties of helium, lithium and O_2. It also accounts in ordinary space for discrete detection. Second, it gives a quantitative map of continuous-matter alternatives that fail these tests, thereby identifying the physical components required for a viable model. Third, it derives within the model rules that are ordinarily postulated in quantum mechanics. In particular, the exchange sign is obtained from the geometry of the body without configuration space, given that an exchange adds no common phase. The absence of self-repulsion follows from the same exchange rule, and detection odds equal to the matter share follow from a stated premise rather than a postulated rule. Since the resulting equations coincide with those of quantum mechanics over the regimes considered here, including the Dirac form of the fine structure, the leading radiative corrections and the spin singlet, agreement with known measurements should be regarded primarily as a consistency test. Accordingly, we propose VRCM as a candidate physical theory grounded in a physical medium, not in a state vector, and not merely as an interpretation. Entanglement, gravity and the regimes in which VRCM may depart from established theory are left for future work.

METHODS

Model and premises: VRCM treats the vacuum as a resonant medium, the nucleus as a compact 1/r source, and electronic matter as one continuous, stationary body that vibrates within the vacuum's trapped resonances and extends into a microscopic fourth spatial direction, *w*. Each ingredient that is assumed rather than derived is stated as a premise where it is first used, and results that depend on a premise are marked as such. Where the model's mathematics coincides with an established theory, this is stated, and the contribution of the model is then its physical reading.

Computation: All calculations were carried out in Python (NumPy and SciPy) in Google Colab. Bound vibration patterns were found by integrating the radial equations with high-order adaptive solvers at tight tolerances and matching the inward and outward solutions;

many-portion systems were solved self-consistently on radial grids; capture and detection were modelled by stochastic simulations with fixed random seeds. Energies are given in hartree (E_h) unless stated otherwise. Physical constants are from CODATA 2022.

Test protocol: Every test was specified with numerical pass/fail criteria before it was run, together with controls designed to fail if the code or the reasoning were wrong, and a stated expectation of the outcome. Results of standard theory were used only to audit numbers, never as premises. When a result disagreed with experiment, the physical description was revised rather than any parameter adjusted. Where a result is marked out of sample, it was computed before comparison with experiment, with every constant fixed beforehand on other systems and nothing refitted.

Calibration and data: Two quantities are calibrated: the action unit Γ of the vacuum's vibration, fixed by measured hydrogen transitions, and the coupling between the two portions of helium-like ions, fixed on helium alone. Measured spectra, magnetic data and scattering limits were taken from the sources cited at each comparison.

Use of software and AI: All Python scripts were reviewed and debugged with the assistance of Claude Code (Anthropic) prior to execution in Google Colab. Grammarly Pro was used to improve language quality and correct grammatical errors. All figures were generated with Python scripts (NumPy and Matplotlib) run in Google Colab. Panels that show results are plotted directly from the script outputs given in the SI (Data S1–S45); schematic panels are identified as schematic in their captions. The figure scripts are available with the other scripts.

RESULTS & DISCUSSION

In the present VRCM model, vacuum is a resonant medium whose vibrations obey the wave rule (eq. 1):

$$\omega^2 = c^2k^2 + \Omega_0^2,\ \Gamma\,\Omega_0 = mc^2 \quad (1)$$

where ω is the angular frequency of a vibration, k its wavenumber, c the speed of light, Ω_0 the vacuum's own vibration frequency, Γ the action unit and m the mass of the electron.

A nucleus at the centre generates a static field in that medium and traps a family of standing resonances. Electronic matter is continuous and stationary. It vibrates in place and settles at the antinodes of the vacuum's trapped resonances. The electronic matter occupies a single three-dimensional body with a Möbius-type half-twist through a microscopic fourth spatial direction, and spin and magnetic moment belong to a two-face

mode of the vacuum that the matter occupies. Unlike traditional configuration space used in Schrodinger's equation, the electronic matter corresponding to each electron is treated as one field over one coordinate. For example, Schrödinger's stationary equation for a helium-like atom with a fixed nucleus is given as (eq.2):

$$\left[-\frac{1}{2}\nabla_1^2-\frac{1}{2}\nabla_2^2-\frac{Z}{r_1}-\frac{Z}{r_2}+\frac{1}{|\mathbf{r}_1-\mathbf{r}_2|}\right]\Psi(\mathbf{r}_1,\mathbf{r}_2)=E\Psi(\mathbf{r}_1,\mathbf{r}_2) \text{ (eq.2)}$$

where $\psi_{(r1,r2)}$ is the joint spatial wave function in six-dimensional configuration space, and Z = 2 for helium. Spin is omitted from the displayed spatial equation; the complete fermionic state must satisfy antisymmetry.

On the other hand, the stationary two-portion *mean-field* equations for VRCM are given as (eq. 3-5):

$$\left[-\frac{1}{2}\nabla^2-\frac{Z}{r}+V_2(\mathbf{r})\right]\phi_1(\mathbf{r})-c_{12}\delta_{s_1s_2}\left(\widehat{K}_2\phi_1\right)(\mathbf{r})=\varepsilon_1\phi_1(\mathbf{r}) \text{ (eq. 3)}$$

The direct electrostatic potentials are

$$V_j(\mathbf{r})=\int_{\mathbb{R}^3}\frac{|\phi_j(\mathbf{r}')|^2}{|\mathbf{r}-\mathbf{r}'|}\,d^3r' \text{ (eq. 4)}$$

and the exchange operators are

$$\left(\widehat{K}_j\phi_i\right)(\mathbf{r})=\phi_j(\mathbf{r})\int_{\mathbb{R}^3}\frac{\phi_j^*(\mathbf{r}')\phi_i(\mathbf{r}')}{|\mathbf{r}-\mathbf{r}'|}\,d^3r' \text{ (eq. 5)}$$

where ϕ_1 and ϕ_2 are the amplitudes of the two portions' vibration, each a normalized pattern in ordinary three-dimensional space with position r; ε_1 and ε_2 are their energies; *Z* is the nuclear charge; V_j is the direct push of portion *j* and $\hat{K}_j$ *its exchange term;* s_i *labels the side (A or B) on which portion i lies, as distinct from the face (+ or −) of the vacuum mode;* $\delta_{s_1s_2}$ = 1 for portions on the same side and 0 otherwise; and c_{12} = 1 when the portions are joined through the connecting necks and 0 when the necks are severed.

Furthermore, atomic energy levels, and hence atomic spectra, are hypothesized in VRCM to arise from nucleus-induced vacuum resonances occupied by continuous electronic matter. The matter's electrostatic self-repulsion is cancelled by its self-exchange term, as in Hartree–Fock theory. Unlike classical magnetic and spin properties, which require moving charge, the present model treats electronic matter as stationary and vibrating locally within a particular resonance pattern. Hence, neither Bohr-van Leeuwen theorem nor the rotating-cloud argument applies in this case. The two portions per pattern follow from the amount of matter a place holds, set by hydrogen, and the face rule, under which the two places of a face share one 3D region separated along *w*. Discrete detection follows from the body contracting onto one place at capture once a detection threshold, taken as a premise, is reached, with odds equal to the share of matter at that place. When two

portions stay joined as one body, the same squeeze carries the spin correlations of separated pairs. The following sections present the step-by-step development of the model.

Geometry and Physical Foundations: What Geometry Can Hold Continuous Matter?

The geometrical and foundational properties of VRCM were evaluated through a series of numerical tests. First, each three-dimensional resonance pattern extends into a fourth spatial direction, giving two folds (C1 and C2) per pattern (Fig. 1B). Further, each fold has two sides (A and B) like the two faces of a Möbius strip.

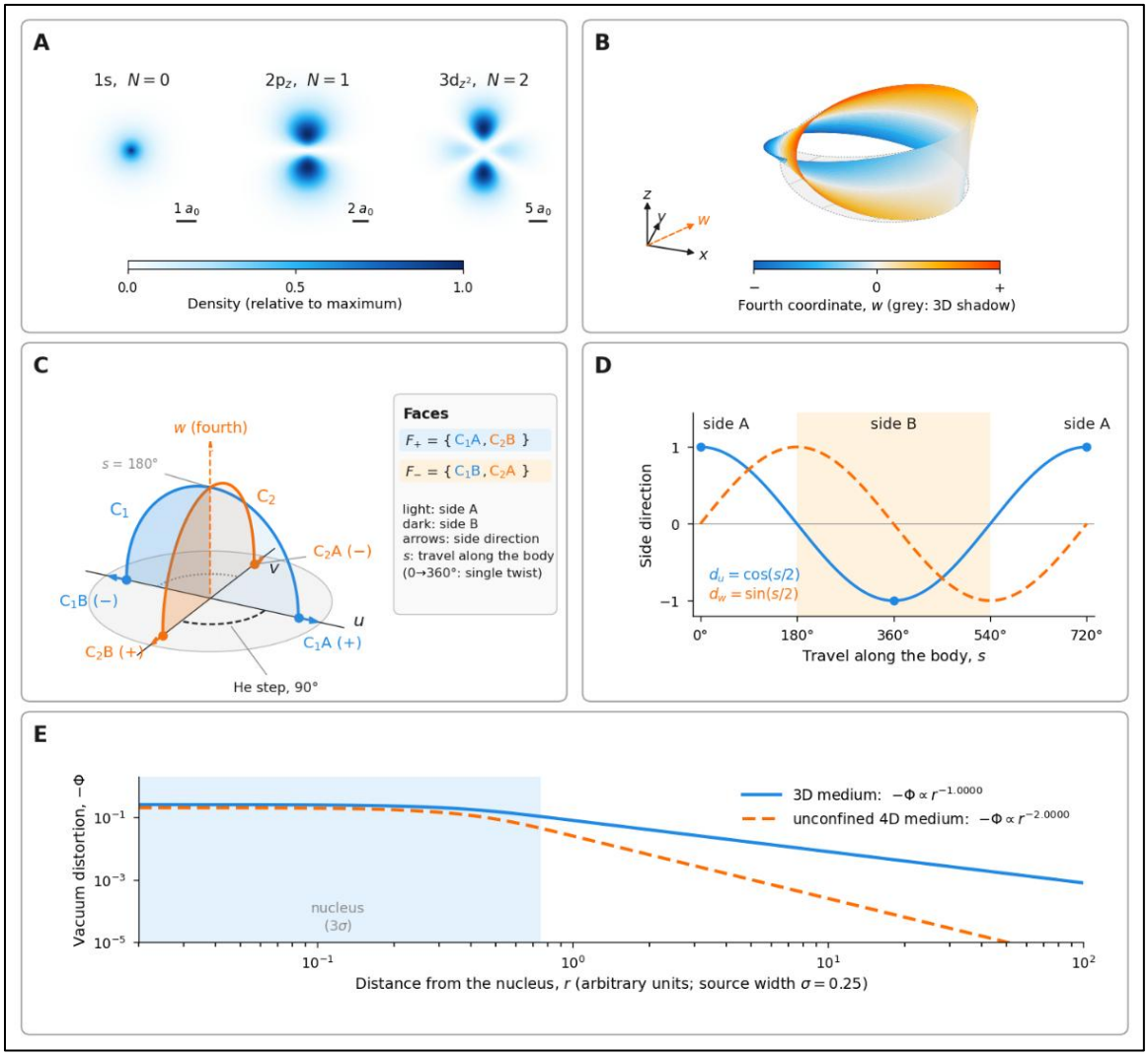

Figure 1. Geometry and foundations. (A) Resonance patterns 1s, $2p_z$ and $3d_{z^2}$. (B) The connected body in four dimensions, coloured by w, with its 3D shadow in grey. (C) Folds C_1 and C_2 and faces $F_+ = \{C_1A, C_2B\}$ and $F_- = \{C_1B, C_2A\}$; the helium

step is 90°. (D) The side direction reverses after one circuit and is restored after two. (E) Vacuum distortion falls as 1/r in a 3D medium and as $1/r^2$ in an unconfined 4D medium.

The results showed that the two folds are enantiomorphs, mirror images of each other with opposite twist handedness but an identical three-dimensional projection (Fig. 1C; See Data S1 in SI). Because the projection is shared, a portion and its partner on the same face (C1A and C2B) occupy the same three-dimensional region and are separated only along *w*. Together they hold twice the matter of C1A in the same volume, whereas the two sides of one fold (C1A and C1B) hold twice the matter in twice the volume (Table 1; see Data S2 in SI). Turning C2 by 90° instead of mirroring it worsened all six term gaps of C, N and O, with the mean second-gap error rising from 13.7% to 32.5% (see Data S3 in SI), so the mirror construction was retained.

Table 1. Volumes of portions of the body relative to C1A.

Portion	Intrinsic volume	Volume of the 3D shadow
C1A	1	1
C1A + C2B (same face)	2	1
C1A + C1B (same fold)	2	2

The ratios are exact for the mirror construction and do not depend on the body's dimensions.

The shared projection is what gives helium room for two portions of matter in one 1s region. Quantum mechanics accommodates the same two units with an internal label instead of a direction in space (Table 2); both give the same ground-state energy and size.

Table 2. Accommodation of two portions of matter in the helium 1s region in QM and in VRCM.

Property	QM	VRCM
What distinguishes two portions in the same 1s region?	Spin, an internal two-valued label	Sides of the mirror folds, separated along the fourth direction w
What limits a pattern to two portions?	Pauli principle (antisymmetry)	One portion per place; two places per pattern share a face
Origin of the sign change when the two are exchanged	Postulated	From the body's reversal after 360° and return after 720°
Space in which the two portions are described	Configuration space, $\psi(r_1, r_2)$	Place labels on one body in three-dimensional space

The first complete circuit (360°) exchanges sides A and B, whereas the second (720°) restores the original orientation (Fig. 1D and eq. 6):

$$\phi(\theta + 2\pi) = -\phi(\theta), \qquad \phi(\theta + 4\pi) = \phi(\theta) \text{ (eq. 6)}$$

where ϕ is the amplitude of the electronic matter's vibration and θ is the angle travelled around the body.

All nine geometrical checks met the predefined criteria (See Data S4 in SI). The half-twisted geometry directly gives a non-orientability to the continuous electronic matter, as shown by the reversal of its four-dimensional normal after one circuit, to within 2×10^{-16} (See Data

S5 in SI). This sign reversal provides the geometrical structure required by the two-face law (See Data S5 in SI). However, the component of normal along the fourth spatial direction vanishes at $s = \pi$, preventing the derivation of a constant rest term. As a result, F2 remains a postulate consistent with the proposed geometry.

An important feature of the model is the microscopic extent of the fourth spatial direction that is constrained by high-energy electron scattering at LEP to $w \leq 2.6 \times 10^{-19}$ m, with an associated shift of hydrogen's 1s level below 1×10^{-15} eV (See Data S6 in SI). Atomic spectra alone cannot set this bound, because the shift equals that of a slightly smaller nucleus. The static vacuum response to a finite nucleus reproduced the exterior 1/r potential, with an exterior ratio of 1.0000000014 and agreement with Gauss's law to 1.1×10^{-14} (see Data S7 and S8 in SI). Unlike an unconfined four-dimensional response, which would scale as $1/r^2$ (Fig. 1E), the proposed vacuum exhibits an effectively three-dimensional long-range interaction. Furthermore, the beat-shift coupling reproduced the hydrogen 2p fine-structure splitting of 10,943.7 MHz, 0.23% below the measured value before the anomalous moment is added, whereas the alternative saturating coupling produced an incorrect 2s–2p separation of 58,263 MHz (See Data S4 and S9 in SI).

The geometrical interpretation of atomic states was examined by treating radial and angular nodes to 2π twists of the continuous body. By the 720° rule, each such twist changes the face angle by about π, as observed (See Data S9 in SI). The total twist count, $N = n_r + l = n - 1$, reproduced the $(N + 1)^2$ hydrogenic spatial states with relative energy spreads below 10^{-5} (Fig. 1A; See Data S5 in SI), consistent with the n^2 Coulomb degeneracy.[23]

One-Electron Spectra and the Action Portion: Can a Continuous Body of Electronic Matter Give Hydrogen's Spectrum and Action Portion?

In VRCM, the nucleus generates conditions for standing-wave resonances in the vacuum, and continuous electronic matter occupies these patterns. Consequently, if this is the physical description of the atom, then the calculated resonances should produce the correct atomic energy levels. Hence, the ability of VRCM to reproduce atomic spectra was evaluated using hydrogen (H), helium (He^{+}), and lithium (Li^{+2}). Starting from a finite nucleus, the generated vacuum field and its trapped two-face modes were used to calculate fifteen spectral transitions. With a single calibration using the hydrogen Hα line, the model reproduced all fifteen transitions within 2.9 ppm without additional species-specific fitting (Table 3; See Data S8 in SI). The residual errors followed the expected pattern associated with the omission of Lamb-shift corrections, showing larger deviations for transitions that

involved lower-lying states and with nearly error-free transitions terminating at n = 3. When two-face treatment was applied, the hydrogen 2p fine-structure gave a splitting of 10,943.7 MHz, 0.231% below the experimental value prior to inclusion of the anomalous magnetic moment. In contrast, the non-relativistic treatment exhibited substantially larger deviations, ranging from 17 to 108 ppm for He^{+} and Li^{+2}, indicating the absence of relativistic fine structure.

Table 3. Comparison of calculated spectral deviations from reference values using the two-face and non-relativistic treatments.

Spectral transitions	Two-face model (ppm)	Non-relativistic model (ppm)
H Balmer-α (3→2; calibration)	0.00	0.00
H Balmer (4, 5, 6→2), Paschen-α (4→3)	+0.02 to +0.27	−2.11 to −5.86
H Lyman (2, 3, 4→1)	−2.26 to −2.92	−1.54 to −2.27
He^{+} (3→2, 4→2, 4→3)	−0.89 to 0.00	+16.81 to +40.46
Li^{2+} (3→2, 4→2, 4→3, 5→3)	−2.16 to −0.41	+46.39 to +108.10

Values correspond to the smallest nuclear width used in the integrated spectral calculations. The two-face equations are mathematically equivalent to the Dirac–Coulomb formulation. Some reference ionic levels include theoretical relativistic and QED contributions

The action unit (Γ), which is analogous to Planck's constant (*h*) in connecting the resonance frequency and energy, was in agreement with *h* within ~3 parts per billion (ppb). A common Γ described 15 spectral transitions for one-electron H, He^{+}, and Li^{+2} systems with a relative spread of 0.37 ppm (See Data S8 in SI). Additionally, fitting five independently measured hydrogen intervals (1S–2S, 1S–3S, 2S–4P, 2S–8$D_{5/2}$, and 2S–12$D_{5/2}$; Mohr et al., 2025) with two-face energy levels and one-loop Lamb-shift corrections reduced the relative spread from 5.3×10^{-7} to 1.3×10^{-9}, an improvement of approximately 396-fold (Data S10 in SI). With Γ fixed, the fine-structure constant used throughout this work is:

$$\alpha_{\Gamma} = \frac{2\pi e^2}{4\pi\varepsilon_0 \Gamma c} \text{ (eq. 7)}$$

where α_{Γ} is the fine-structure constant, e is the elementary charge, ε_0 the permittivity of the vacuum and c the speed of light.

The current model does not treat the agreement between Γ and Planck's constant (*h*) as an independent determination of *h;* rather, it is taken that the consistency of Γ across the measured transitions supports the internal consistency of the model's Dirac-equivalent spectral formulation. The remaining deviations showed opposite trends for transitions originating from 1S (≈ +0.6 ppb) and 2S–nD transitions (≈ −0.6 ppb), representing factors that were not accounted for in the current model (see Data S10 in SI).

Origin of Spin, Magnetic Moment, and QED-Level Corrections: Where Do Spin and the Magnetic Moment Come From if Nothing Spins?

Conventional quantum mechanics treats spin as an intrinsic property of the electron, and its magnetic moment as the interaction of that spin with an external magnetic field. While the term spin can be erroneously connected to classical angular momentum, QM describes it mathematically by spinors in the Dirac equation rather than the physical rotation of the electrons. In contrast, VRCM offers a physical description that maintains the established relativistic quantum predictions. In this model, spin is associated with the two-face 3D structure of vacuum resonance modes into 4th spatial dimension, rather than the circulation of continuous electronic matter. The magnetic moment is consequently attributed to vacuum mode, while the continuous electronic matter occupies the corresponding resonance pattern. However, to test whether the origin of spin and magnetic moment involved any circulation of continuous physical matter within vacuum resonance modes, several mechanisms were considered. The VRCM that involved local circulation of matter produced integer winding rather than spin-1/2 behavior (See Data S11 in SI). Furthermore, the dynamic occupation of the two sides of the vacuum resonance mode yielded a Penning-type ratio of ~0.41 instead of 1 (See Data S12 in SI). Similarly, assigning magnetic moment to a ring-shaped continuous electronic matter around the nucleus gave an incorrect Zeeman shift (0.65 per unit) and the state multiplicity ([2, 2, 2] instead of [1, 1, 1]; See Data S13 in SI). Matter carried around the pattern was therefore excluded, but matter vibrating in place was not: the lowest two-face vacuum mode is a degenerate pair of winding ½, and a circular local vibration of the matter within it, with no transport of matter, carries a moment that an applied field selects (See Data S14 in SI). Assigning the magnetic moment to the vacuum's two-faced 3D-structured mode oriented in the 4th spatial direction reproduced the expected spin quantum number ($J = ½$), with $g = 1.999964499$ for the bound 1s state and $g = 2$ to within 10^{-12} in the free limit (See Data S4 and S15 in SI). Furthermore, the helium singlet normal Zeeman pattern was reproduced, yielding shifts of $\pm\mu_B B$ to within 10^{-6}, with one state per component (See Data S15 in SI). These findings demonstrate that the two-face vacuum-mode formulation is consistent with the tested magnetic properties, whereas the examined matter-circulation mechanisms were not.

Next, the electron's anomalous magnetic moment was tested. Dirac's equation predicts the electron's magnetic g-factor as exactly 2. However, experimentally it is shown to be slightly higher due to quantum electrodynamics effects. The VRCM reproduced the QED correction, $F_2(0) = \alpha/2\pi$, within 1.7×10^{-7}, and gave the value of 0.0011614, which is ~0.15% above the measured value 0.00115965. The corresponding Pauli term increased

the hydrogen 2p fine-structure splitting by the expected factor 1 + 2a, with agreement within 0.1% (See Data S16 in SI). Furthermore, in conventional quantum electrodynamics, the vacuum polarization, arising from virtual electron–positron fluctuations, modifies the electromagnetic field around the nucleus. For VRCM, this correction using relativistic field formulation reproduced the Uehling potential within 10^{-8}, lowering the hydrogen 2s energy level by 27.08 MHz (See Data S17 in SI).[24] These same quantum radiative effects account for the Lamb shift, a small energy difference experimentally observed between the $2s_{1/2}$ and $2p_{1/2}$ levels of hydrogen. These levels were supposed to be degenerate as per the Dirac theory. While the anomalous magnetic moment and vacuum polarization tested the electron's interaction with the vacuum field in the current model, the Lamb shift tests how vacuum fluctuations modify the energies of atomic electronic patterns. Thus, after computing the vertex and vacuum-polarization sectors independently, we examined VRCM's ability to reproduce the Lamb shift and its underlying physical mechanism.

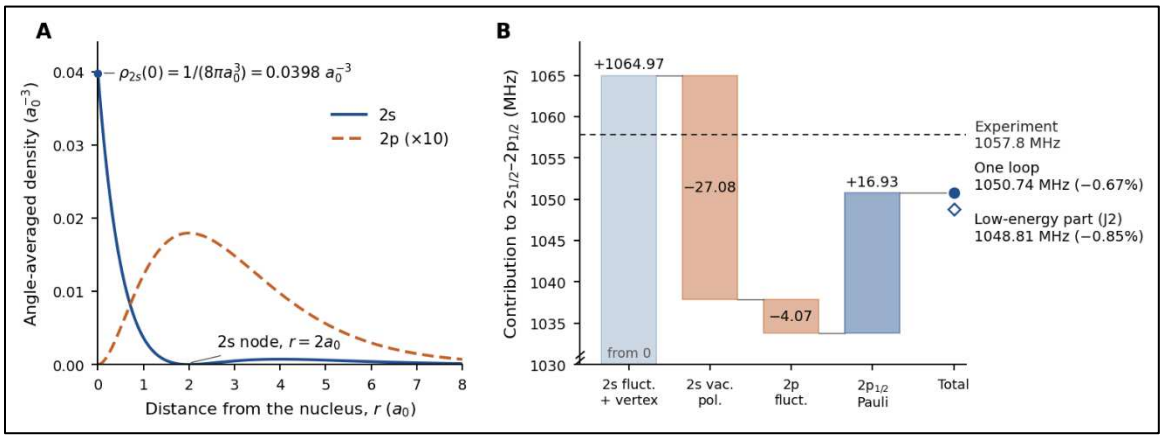

Figure 2. Plot showing hydrogen electron densities and Lamb-shift contributions. (A) Angle-averaged 2s and 2p densities, showing the finite 2s density at the nucleus and its radial node at $2a_0$ (2p scaled ×10). (B) One-loop contributions to the $2s_{1/2}$–$2p_{1/2}$ splitting, yielding 1050.74 MHz (−0.67%) versus the experimental 1057.8 MHz. The separate low-energy response calculation gives 1048.81 MHz (−0.85%).

In VRCM, the Lamb shift has a simple origin. Zero-point vibrations of the vacuum field displace the continuous matter by about 0.07 pm, so the matter feels the nuclear attraction smeared over that distance. The smearing becomes important only where the attraction changes sharply, at the nucleus. The 2s pattern, which has matter there, is therefore raised much more than the 2p pattern (Fig. 2A; See Data S18 in SI). To obtain the size of the shift, the pattern equations were driven at each frequency and solved directly, without importing Bethe logarithms (See Data S19 in SI). The response of the free electron was subtracted, and the sum over vacuum modes was cut at the vacuum frequency Ω_0, where $\hbar\Omega_0 = mc^2$. The resulting Bethe logarithms were 2.811451 for 2s and –0.030020 for 2p, which were close to the published values of 2.811770 and −0.030017.[25] From these

calculated responses, the 2s level increased by 1052.88 MHz whereas the 2p level by 4.07 MHz, producing a Lamb shift of 1048.81 MHz (Fig. 2B). This value lies 0.85% below the experimental 1057.8 MHz (Fig. 2B). Since the high-energy relativistic part and vacuum polarisation were not incorporated in the calculations, the estimates reflect only the low-energy component of the shift.

The full one-loop calculation combined the low-energy fluctuations with the high-energy relativistic vertex corrections, giving a Lamb shift of 1050.74 MHz, 0.67% below the experimental value (Fig. 2B; See Data S20 in SI). The low-energy response follows from the model's own pattern equation and vacuum modes, although its mathematics is the same as that of non-relativistic QED. The high-energy vertex was computed with the structure of QED, using the two-face matrices, and deriving it from the vacuum dynamics of VRCM remains an open problem.

Two Portions Without Configuration Space (He & He-like Species): How do two portions share one atom without configuration space?

Systems with more than one portion are where VRCM differs significantly from the standard description. In traditional QM, a joint many-electron wave function in configuration space describes multi-electronic systems. In contrast, the VRCM describes electronic matter as one continuous body occupying resonance patterns, analogous to matter occupying a resonating Chladni plate. Each resonance pattern had four labelled places (C1A, C1B, C2A and C2B) which represent two folds and two sides of the connected body. The amount in each portion is described by a density over a single position in ordinary space. For Li, positioning the third portion of electronic matter on the same face in 2s is energetically favored. One-dimensional tests showed that the same-face rule not only lowered the energy by 0.158 Ha, but without it the third portion collapsed into 1s with an error of 35.7 eV (See Data S1 and S9 in SI). The first ionization energy of lithium comes out at 5.409 eV with the collective vibrations included, compared to the experimental value of 5.392 eV (See Data S1 in SI). With the 2s pattern kept free of 1s matter, lithium's 2s lies below its 2p, and the 2s–2p gap comes out at 14,453 cm^{-1} which is within 3.1% of the measured (14904 cm^{-1}; See Data S21 in SI). The exchange sign, $(-1)^{2s}$, is not assumed but follows from the geometry of the electronic body. Moving along any path on this body, the sign reverses after one circuit and is restored after two, in both folds, C1 and C2. Because the patterns are joined in one connected body, the exchange term also acts between them, through the necks where same-side matter of two patterns overlaps: O_2-type pair then gives the spin-only moment of 2.828 μ_B and paramagnetic susceptibility within 0.5% of the experimental value. On the other hand, the model with severed portions gives 2.449 μ_B and misses the

susceptibility by 25.5% (See Data S1 in SI). In helium, the two portions are locked in one opposite-side arrangement with total spin zero ($\langle S^2 \rangle = 0$), so helium is purely diamagnetic, and its susceptibility lies 0.7% below the experimental value (See Data S9 and S22 in SI). Helium's correlation energy, where the first route overshoots, is treated below.

Hydrogen sets the amount of matter a place holds. Each place holds at most one hydrogen-equivalent of matter, so twice the matter needs twice the places. Helium gains them by folding into the fourth spatial direction, w. Its two places, C1A and C2B, share one three-dimensional region and are separated only along w (Table 1), so helium does not expand but in fact is smaller than hydrogen ($\langle r^2 \rangle = 1.18\ a_0^2$ per place's worth against $3\ a_0^2$; See Data S23 in SI). The matter stays on the same face on which it starts, and distance along the body orders the places on that face (See Data S24 in SI). Helium's second portion therefore takes C2B, 90° along the body, with the opposite spin. Moving on to lithium, its third portion enters 2s (720°) rather than the back face of 1s (360° and 450°). With no separate capacity rule, this gives the measured shells and spin multiplicities from H to Ne, and each pattern closes at two portions of opposite spin, which reproduces the Pauli limit (Fig. 3A, C; See Data S24 in SI). However, if the ranking is solely based on rotational angle, then carbon, nitrogen and oxygen break Hund's first rule. On the other hand, ranking based solely on distance along the body sends lithium's third portion into 1s, where it would miss the energy by 35.7 eV.

The premise can also be stated in terms of space. For example, the two places of the same face (C1A and C2B) occupy the same 3D points, keeping electronic matter of a particular pattern in one 3D shadow, while the opposite face would double the space the pattern occupies (Table 1). Filling by that rule reproduces the face rule for place in every branch from H to Ne, and neon's ten portions occupy five shadows, one face of each pattern (See Data S25 in SI). However, trying to conserve 3D space fails instead: lithium's third portion then goes to the backside of 1s, which is nearer than 2s, giving $1s^3$ and then $1s^4$. As a result, conserving 3D space holds for pattern but not for the atom as a whole. The face rule is therefore a geometric premise governing how a pattern occupies space: hydrogen sets the amount each place holds, and the limit of two per pattern follows from the face rule, since a face has only two places.

To test how much w contributes to helium's binding, the two portions of helium were prevented from sharing any three-dimensional point in three different ways, without correlation in any case (Fig. 3A). A helium system in which the electronic matter is arranged in two hemispheres within the same 3D space separated by a plane through the nucleus lies 34 eV above He^+. Such a system cannot hold its second portion. The arrangements where electronic matter is separated into inner and outer regions, or best spatially

disjointed regions, are ~20 eV higher than He with shared electronic matter and only ~3 eV lower than He^+. Additionally, these two arrangements led to expansion of the He atom by a factor of 16 to 27 in terms of $\langle r^2 \rangle$ (Fig. 3C). Among the three arrangements, only the fold in which two portions of electronic matter shared one 3D region that is separated along w gave a compact and strongly bound ground state of helium. This arrangement accounts for ~85% of the energy that holds the second portion of He relative to the tested non-overlapping arrangements (See Data S26 in SI). Interestingly, a ~20 eV energy penalty is comparable to the 19.82 eV excitation energy separating helium's 1s2s triplet state from its ground state, although the underlying spatial constraints differ. Thus, in VRCM, separation along the fourth spatial direction, *w*, allows two portions of continuous electronic matter to share one three-dimensional projection, analogous to the occupation of the same 1s orbital by electrons of opposite spin in quantum mechanics.

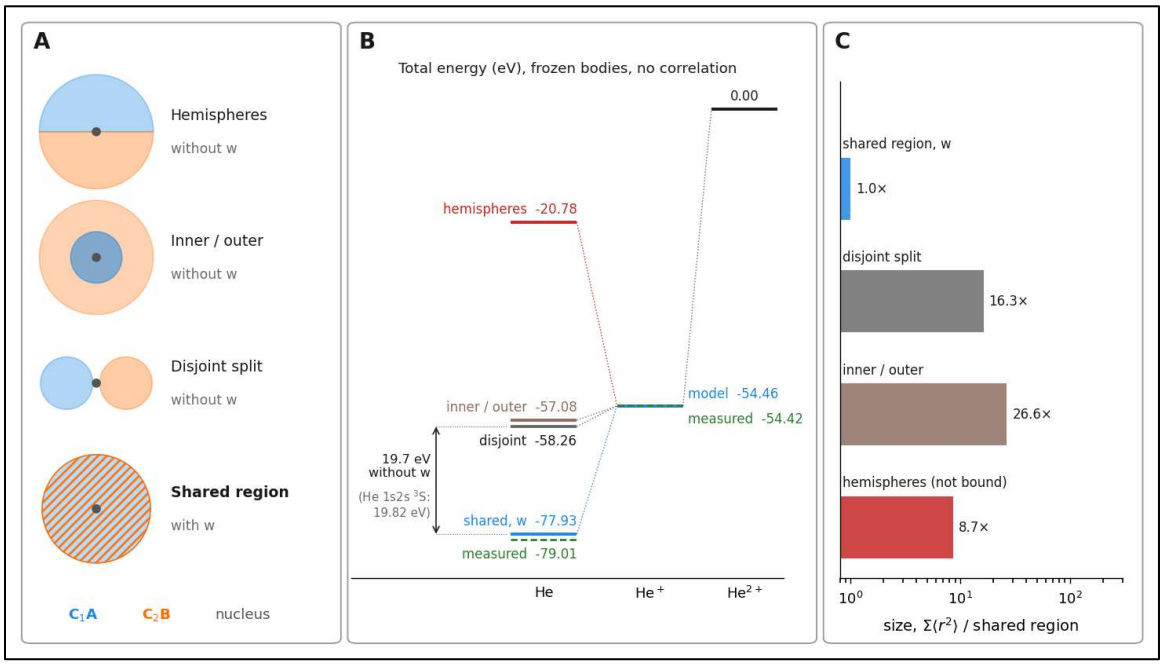

Figure 3. Helium with and without w. (A) Four ways of placing helium's two portions, C_1A (blue) and C_2B (orange). The first three keep them apart in 3D (hemispheres, inner/outer regions, disjoint split); the last has them share one 3D region, separated along w. (B) Total energies of the frozen bodies, without correlation, with measured values for comparison. Removing w costs about 20 eV, comparable to the He 1s2s ^3S excitation (19.82 eV). The hemisphere arrangement cannot hold the second portion. (C) Size, $\Sigma\langle r^2 \rangle$, relative to the shared region. Model energies carry a grid uncertainty of about 0.06 eV.

Next, the electronic matter at the necks, the regions where the two patterns join, was investigated. Severing the body at the necks removes the exchange term between same-side portions in different patterns. As a result, the paramagnetic moment of O_2 drops from 2.828 to 2.449 μB, and the error in frozen-body ionization energy of lithium grows from −0.049 to −0.116 eV (See Data S1 in SI). Here, the preference for the same side emerges

from the exchange term, which is positive for any pattern shape because the Coulomb push is positive-definite (See Data S17 in SI).

Turning to correlation, VRCM's results were compared with two methods from standard theory. Without vibrations, the connected body reproduces a standard mean-field energy to within 2×10^{-10} Ha (See Data S1 in SI). With vibrations, its mathematical treatment matches the ring (RPA) treatment of Bohm and Pines, limited by the turn rule.[26]

Although the collective vibrations in VRCM capture most of helium's correlation, its small-vibration treatment overestimates the correlation stabilization by 16.2%. To test whether this overestimation was an artifact of geometry or had to do with nuclear charge, the same code that gave 16.2% higher correlation for helium was applied to the two-portion series H^-, Li^+ and Be^{+2} by keeping everything unchanged except for the nuclear charge Z (Table 4). With the vibrations of electronic matter treated as local gentle movements around its resting state, the extent to which correlation overshoots drops from 16.2% in He to 9.7% in Li^+ and 6.9% in Be^{+2}. As for H^-, the nucleus was too weak to hold the vibrating body steady. With the capacity limit, the model overestimates correlation in H^-, He, Li^+, and Be^{+2} by 1.6%, 13.6%, 8.8%, and 6.4%, respectively (See Data S27 in SI). These results show that the overestimation is not a fixed percentage error, as its magnitude shrinks with increasing Z. As shown below, the absolute correlation-energy overestimation falls as 1/Z, and it is consistent with missing contribution from the short-range encounters of the two portions.

When a capacity limit was imposed on vibrating matter, the product of overestimation and Z gives 0.01145, 0.01145 and 0.01138 E_h for He, Li^+ and Be^{+2}, respectively. This corresponds to a residual of approximately 0.0114/Z E_h within 0.6% (See Data S28 in SI). Thus, when correlation energy is expressed as ($a + b/Z$) and fitted to He, Li^+ and Be^{+2}, VRCM's capacity-limited vibrations gave $a = -0.04644$ E_h, closely matching the value obtained by fitting reference data for the same three ions ($a = -0.04647$ E_h) and approaching the independently calculated QM-limit -0.04666 E_h at infinite nuclear charge. However, the model gave $b = -0.00265$ E_h compared to $+0.00887$ E_h obtained from the reference fit. This leading term is the second-order correlation energy, which any treatment correct to second order reproduces; without the turn rule, the same vibrations give 198.4% of the needed correlation in He, twice the needed value (See Data S9 in SI). Thus, collective vibrations of the continuous matter capture the leading correlation contribution without configuration space, while the residual occurs at the next order, consistent with missing short-range interactions analogous to ladder corrections in many-body theory.

Table 4. Correlation of the two-portion series from H^- to Be^{+2} with small and capacity-limited vibrations.

Atom	Small vibrations	Capacity-limited	Total energy (E_h)	Exact (E_h)	Miss
H^-	unstable (1 mode)	+1.6%	–0.528390	–0.527751	–0.017 eV
He	+16.2%	+13.6%	–2.909435	–2.903724	–0.155 eV
Li^+	+9.7%	+8.8%	–7.283669	–7.279913	–0.102 eV
Be^{+2}	+6.9%	+6.4%	–13.658250	–13.655566	–0.073 eV

% are the excess of the model's correlation over the needed correlation (exact minus Hartree–Fock limit).[27,28,29] Total energies include the capacity-limited vibrations; miss = model – exact.

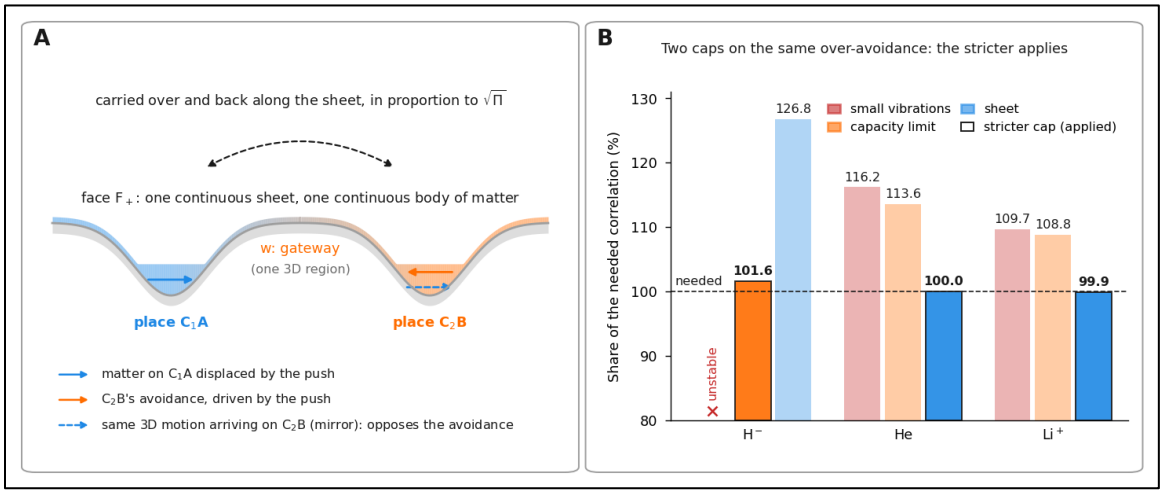

Figure 4. The coupling between C1A and C2B, and the stricter-limit rule. (A) One continuous body of electronic matter spans places C1A and C2B of face F_+, which share one 3D region and are separated only along w. A push-driven vibration on C1A is carried along the body (in proportion to $\sqrt{\Pi}$) and arrives on C2B as the same 3D motion, opposing its avoidance. The coupling strength κ is fixed on helium, and its range is the pattern's density fall-off length. (B) Share of the needed correlation for H^-, He and Li^+. The capacity limit and the coupling cap the same over-avoidance, and the stricter applies (outlined bars). Applying both to H^- double counts (82.7%).

The remaining residual in correlation energy was examined by testing coupling vibrations between C1A and C2B, the two portions of continuous electronic matter connected through the 4th spatial direction, *w*. This coupling interaction between the two portions prevents an excessive decrease in energy by counteracting correlation stabilisation. First, the overestimation of helium was corrected by introducing a coupling constant, κ, which reflected how vibrations were transmitted from C1A to C2B (Fig. 4A). Using this constant, fixed on helium alone, the model recovered 99.9% of the required correlation energy for every helium-like ion from Li^+ to Ne^{+8}, including the six ions from B^{+3} to Ne^{+8} that were not used to fix anything, and 101.6% for H^- (Fig. 5A). This correlation energy gave a = –0.04640 E_h and b = +0.00873 E_h, values close to the reference fit (a = –0.04647 and b = +0.00887 E_h, Fig. 5B). For H^-, the capacity limit provided the more restrictive correction, recovering 101.6%, whereas combining both corrections reduced the recovery to 82.7% (Fig 4B; See Data S29-S31 in SI).

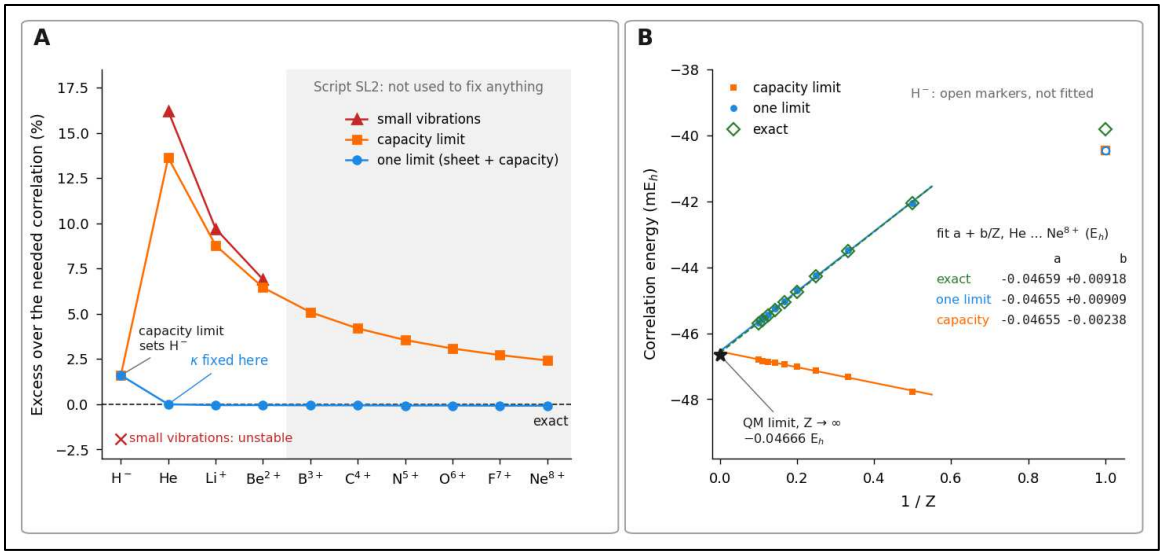

Figure 5. Correlation along the helium-like series. (A) Excess of the model's correlation over the needed correlation, from H^- to Ne^{+8}. κ is fixed on helium only; the shaded ions were not used to fix anything. (B) Correlation energy against 1/Z, with a + b/Z fitted from He to Ne^{+8} (H^- open, not fitted). Only the one-limit rule reproduces the exact a and b. The star marks the limit at infinite Z.

Second-Row Ground Terms and Hund's Rule: Do They follow from the geometry?

In conventional atomic physics, spin-orbit coupling further splits atomic terms into closely spaced levels with different J values, where allowed. In VRCM, the sign is set by the two-face law and is fixed on hydrogen. Now, the second row was treated with the same rules as helium and lithium, in conjunction with the sign set by the two-face law (Section 2.3) .

$$\Delta E_J = \frac{A}{2}[J(J+1) - L(L+1) - S(S+1)] \text{ (eq. 8)}$$

where ΔE_J is the shift of the level with total angular momentum J from the centre of its term, A is the coupling constant of the term, L is the total orbital angular momentum and S the total spin of the term.

$$\xi(r) = \left(\frac{\alpha^2}{2}\right)\left(\frac{1}{r}\right)\left(\frac{dV}{dr}\right) \text{ (eq. 9)}$$

where $\xi(r)$ is the spin–orbit strength at distance r from the nucleus; α is the fine-structure constant (≈ 1/137); r is the distance from the nucleus; V is the potential in which the portion moves (−Z/r for the bare nucleus); dV/dr is its radial gradient in a.u.

As a result, the model correctly gave the lowest levels for B (J = 1/2), C (0), N (3/2), O (2) and F (3/2) (See Data S32 in SI). The two control studies further corroborated that this agreement did not arise by chance. In the first control, reversing the sign of the coupling inverts the order of the levels and gives the wrong lowest J for B, C, O, and F. Nitrogen stays

unaffected because its ^4S ground term is a single level. In the second control, when the exchange sign associated with the connecting necks was removed, the model predicts an incorrect ground term for C (^1P), N(^2S) and O(^1S) instead of the actual ^3P, ^4S and ^3P states, respectively. The electrostatic repulsion between portions alone therefore does not give Hund's first rule; it follows from the exchange sign supplied by the geometry of the connected body.

With the degeneracy premise, the VRCM recovers the mathematical formulation of Slater-Condon multiplet theory (Slater 1929; Condon and Shortley 1935).[30,31] Thus, the contribution of VRCM lies in the physical interpretation of atomic terms as stationary modes of one continuous body of electronic matter, without invoking a conventional many-electron wave function in configuration space. The calculated ground state terms for all 21 tested species from Li to Ne, which included cations and anions, not only agree with experimental data but also reproduce the observed ordering under Hund's three rules (Table 4; See Data S32 in SI). With the same patterns used for all terms, the calculated ratio of the two term gaps is 2.50 for C and O and 1.67 for N, compared with the experimental values of 2.12, 2.13 and 1.50, respectively. For C, N, and O, the first-term gaps agree with experimental results within 1.6-10%, whereas the second gaps are overestimated by 19-30% (See Data S33 in SI). These deviations may arise from term-specific pattern relaxation and correlation effects, examined below.

In addition to deciding the capacity of each pattern and which places are occupied within it, the face rule also contributes to the order within the 2p shell. As electronic matter fills 2p, each new portion faces a tie: on the front face, a step to the other fold of the same pattern is 90° along the body, whereas a turn into a new p pattern is also 90°. In conventional QM terms, it would be analogous to having two electrons in the same orbital vs. two unpaired electrons in different 2p orbitals. In the case of VRCM, the tie is decided by the electrostatic repulsion minus the same-side exchange. Positioning the new portion of the continuous body in the same pattern as the existing one places both in one 3D region on opposite sides, with the full electrostatic repulsion and no exchange. However, placing it in a new pattern on the same side is energetically favorable, as it not only lowers the electrostatic repulsion but also adds the trade through the neck. Thus, from boron to nitrogen, the electronic matter fills in px, py and pz at C1A, each a 90° turn from the last. From oxygen to neon it pairs through the helium step C1A→C2B. The measured multiplicities of B, C, N, O and F (2, 3, 4, 3, 2) come out in all 144 branches of the remaining choices (Fig. 3A, C; See Data S24 in SI). The outcome is the same as in conventional QM, but the origin of each step differs. In QM, the limit of two electrons per orbital follows from the antisymmetry of the wave function, the competition between pairing and a new orbital from their degeneracy, and the exchange integral from antisymmetry, with no classical

counterpart. In VRCM, this limit follows from the two places of a face, the competition from two equal steps along the body, and the exchange from a physical trade of matter through the neck between same-side patterns. In both descriptions, however, the lower energy of the triplet comes mainly from contraction towards the nucleus rather than from reduced repulsion, as shown below for helium and as found in conventional calculations.[32]

Table 5. Singlet and triplet 1s2p states of helium: model and experiment.

Quantity (He 1s2p)	Model	Experimental	Difference
Order of states	$2^3P < 2^1P$	$2^3P < 2^1P$	same
$2^1P - 2^3P$ splitting	0.2442 eV	0.2539 eV	−3.8%
Binding of the 2p portion, 2^3P	3.5765 eV	3.6233 eV	−0.047 eV (−1.3%)
Binding of the 2p portion, 2^1P	3.3323 eV	3.3694 eV	−0.037 eV (−1.1%)
2p size ⟨r⟩, 2^3P	4.656 a_0	not measured	—
2p size ⟨r⟩, 2^1P	5.141 a_0	not measured	—
Triplet − singlet, nuclear pull	−0.040 E_h	—	(mechanism)
Triplet − singlet, push	+0.022 E_h	—	(mechanism)

To investigate the physical origin of Hund's first rule in VRCM, the singlet and triplet excited states of He (1s2p) were relaxed separately. In the triplet, both portions lie on the same side and trade through the neck joining the 1s and 2p patterns, whereas the singlet is the AB/BA mode, in which the two arrangements with the portions on opposite sides resonate together. The model not only gave the correct singlet-triplet order but also reproduced the splitting that was only 3.8% off the experimental value and the binding of the 2p portion within about 1% of the experimental value (Table 5; See Data S33 in SI). The model attributes the lower energy of the triplet to the exchange through the necks that leads to contraction of electronic matter towards the nucleus.

With VRCM reproducing Hund's first two rules from its geometry— the first from the exchange sign of the connected body, and the second from the half-angle push along the body, which gives the order $^3P < ^1D < ^1S$ without the multiplet coefficients of the standard theory—Hund's third rule was investigated. In standard QM, the spin-orbit coupling splits the ground term into different J levels. The third rule states which J is the lowest, based on the sign of the spin-orbit coupling projected onto the ground term. In VRCM, spin comes from the side a portion sits on (A or B), and the angular part from the shape of the pattern. Thus, spin and magnetic moment originate from the two-face vacuum mode the continuous body of electronic matter occupies. The two-face law then determines the strength and sign of coupling and was tested on hydrogen.

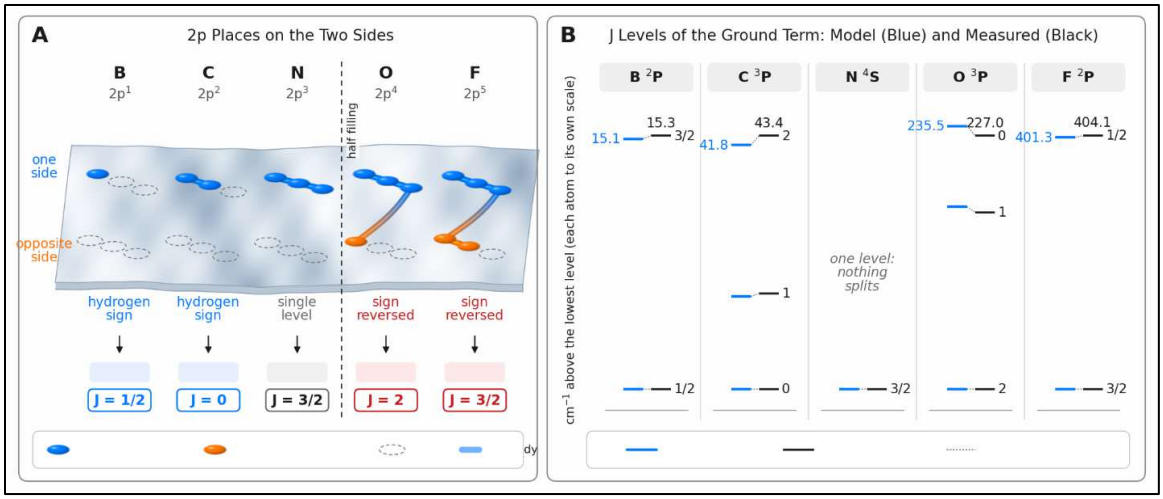

Figure 6. Order of the J levels in the ground terms of boron to fluorine. (A) 2p places on the two sides. (B) J levels of the ground terms, model (blue) and measured (black), in cm^{-1} above the lowest level, each atom on its own scale.

The order of J levels then depends on how the 2p portions fill the two sides. The sign does not reverse as long as the side is retained. In boron and carbon, the 2p pattern contains one and two portions on the same side, leaving space for one more portion (Fig 6A). Under the two-face law, the coupling keeps its hydrogen sign, giving boron and carbon the lowest J of 1/2 and 0, respectively. In the case of nitrogen, one side is fully occupied by a continuous body of electronic matter, giving it a ground term (^4S) that has only one J level (3/2), so nothing splits and there is no order to decide. The sign reverses in oxygen and fluorine, where the shell is more than half full and the extra portions occupy the opposite side. As a result, the order in oxygen and fluorine inverts (Fig. 6A & 6B; See Data S33 in SI).

Fine Structure: What Sets the Size of Splitting?

With the order of the J levels set by how 2p portions are filled on two sides, the size of splitting is governed by the two-face law, which acts not only between each portion and the nucleus but also between the portions of the continuous body of electronic matter in three different ways (Fig. 7A & B). First, the electrostatic repulsion from the other portions of the continuous matter opposes the nuclear pull and weakens coupling between each portion's side and its shape. Second, the shape of each portion's pattern acts on the sides of the other portions, which weakens the splitting further. Third, the sides of different portions couple to each other.

Interestingly, the way the vacuum vibrates a pattern sets the strengths of these couplings, and the placement of the matter within a pattern decides their sign and size. With the patterns shaped by the pull, the push and the same-side trade through the necks, out of

three tested vibrations, only the one in which the whole pattern vibrates at once, with the empty and filled places at the same strength, reproduced helium's level order and gave splittings for B, C, O and F within 1.3%, 3.7%, 3.8% and 0.7% of measured values (15.1, 41.8, 235.5 and 401.3 cm^{-1} against 15.3, 43.4, 227.0 and 404.1 cm^{-1}), with interval ratios of 1.63 for carbon and 0.44 for oxygen against the measured 1.65 and 0.43 (Table 6; Fig. 7C; See Data S34 in SI).

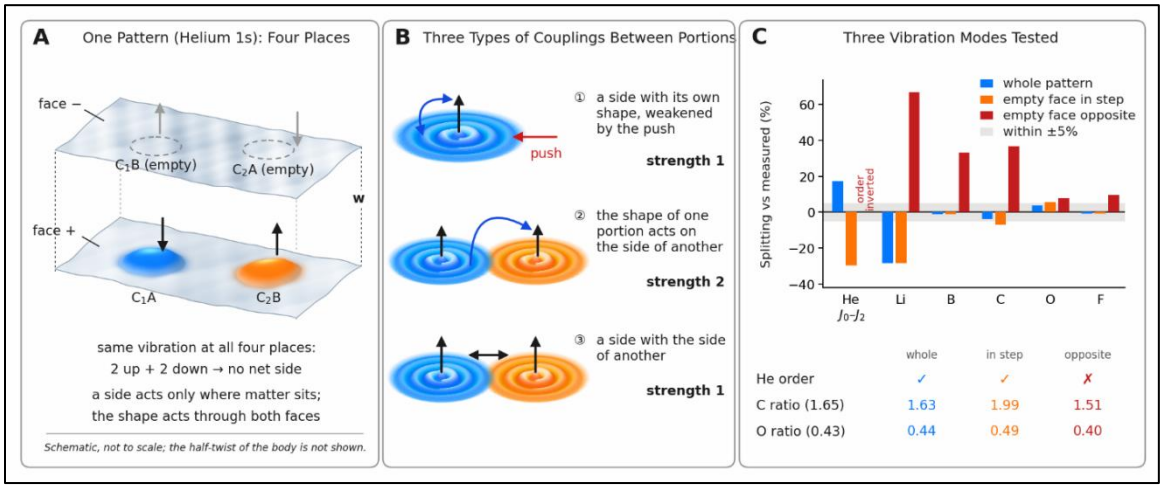

Figure 7. Fine structure from the vibration of the whole pattern. (A) The four places of the helium 1s pattern on faces + and − (schematic, not to scale). (B) The three couplings between portions. (C) Splittings relative to measured values for the three vibration modes of the empty face (whole pattern, in step, opposite), with helium's level order and the interval ratios of C and O.

Table 6. Fine-structure intervals (cm^{-1}) of He 2^3P, Li 2p and the ground terms of B, C, O and F for the three tested ways the vacuum vibrates the pattern, with the interval ratios of C and O.

	He 2^3P_0–2^3P_2	He 2^3P_1–2^3P_2	Li	B	C	O	F	C ratio	O ratio
Measured (cm^{-1})	1.064	0.076	0.335	15.29	43.40	227.0	404.1	1.646	0.434
Whole pattern	1.249	0.166	0.240	15.09	41.78	235.5	401.3	1.632	0.442
In step	0.749	0.499	0.240	15.09	40.36	239.6	401.3	1.987	0.492
Opposite	order inverted	order inverted	0.559	20.35	59.31	244.7	443.1	1.510	0.396

Since each pattern has four places (C1A, C1B, C2A, and C2B) carrying equal numbers of opposite spin labels, the vibration of the whole pattern has no net side; a side acts only at a place that holds matter (Fig. 7A). The shape, however, is the same at every place, so a portion's shape acts through both faces of its fold. The second coupling is therefore twice as strong as the first, and the third remains. Furthermore, when a magnetic field is introduced into the two-face law, without assigning magnetic moment to either side, each side responds with gs = 2 while the electronic matter remains at rest (See Data S35 in SI). Unlike conventional atomic physics, where this value follows from the mathematical

structure of the spinor in Dirac's theory, VRCM offers a physical picture of its origin: the coupling between the two faces of the vacuum mode, with the electronic matter at rest. With G and F denoting the matter on face + and face –, this two-face law reads:

$$\frac{dG}{dr} = -\frac{\kappa}{r}G + \frac{E+mc^2-V(r)}{\hbar c}F \text{ (eq. 10)}$$

$$\frac{dF}{dr} = \frac{\kappa}{r}F - \frac{E-mc^2-V(r)}{\hbar c}G \text{ (eq. 11)}$$

where G and F are the amplitudes of the electronic matter's vibration on face + and face −, r is the distance from the nucleus, κ labels the pattern (κ = –1 for $s_{1/2}$, +1 for $p_{1/2}$, –2 for $p_{3/2}$), E is the energy, V(r) is the potential of the nucleus, m is the mass of the electron, c is the speed of light and ħ = $\Gamma/2\pi$.

The equations 10 and 11 have the form of Dirac's radial equations, with κ labelling the pattern; VRCM reads their two components as matter on the two faces of one body. The two alternative modes of vibration, with the empty face vibrating in step or opposite to the occupied one and each carrying a side, were tested and rejected. The in-step vibrations return carbon's interval ratio to 1.99 and make helium's 2^3P_1–2^3P_2 interval six times too large. The opposite vibrations invert helium's level order and overestimate Li, B and C by 33–67% (Table 6; Fig. 7C; See Data S34 in SI).

Electrostatic Sign, Self-Interaction and Two Kinds of Charge: Why Do Like Charges Repel?

In conventional atomic physics, when the electron is treated as a particle, Coulomb's law fixes the sign of the force, the self-term is left out of the Hamiltonian, and charge is assigned to each particle. However, a model in which the electron is treated as a continuous body of matter cannot assume it. Instead, it must be able to derive 1) why the field between like sources is repulsive, 2) why continuous matter does not repel itself, and 3) why charge comes in two kinds. After having established the geometric and spectral properties of the continuous-matter model, we tested whether VRCM can answer these three questions.

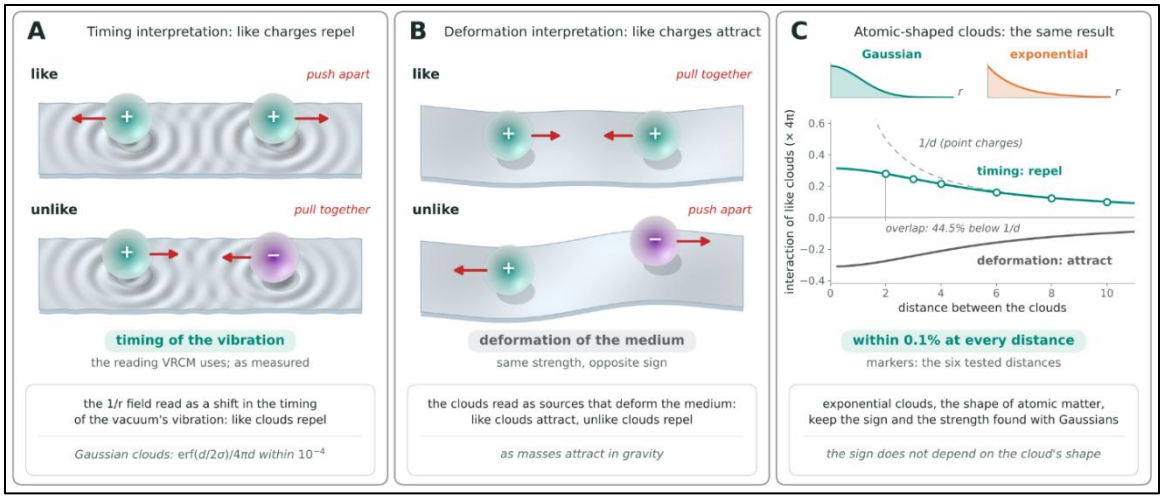

Figure 8. Sign of the force between like charges. (A) With the 1/r field interpreted as a shift in the timing of the vacuum's vibration, like clouds repel and unlike clouds attract. (B) Interpreted as sources that deform the medium, the same clouds give the same strength with the opposite sign: like clouds attract, as masses do in gravity. (C) Interaction of like clouds (× 4π) against distance for Gaussian and exponential clouds.

First, to address the sign of the force, two smooth clouds of charge were considered to mimic the continuous body of electronic matter whose charge is spread over its pattern. These clouds were placed at several distances from each other, and the static energy was calculated for each distance using the field equation. When the 1/r field is interpreted as a shift in the timing of the vacuum's vibration, like Gaussian clouds repel and unlike clouds attract with the full 1/r strength. The magnitude of their interaction then equals the closed form $\mathrm{erf}(d/2\sigma)/(4\pi d)$, where σ is the width of each cloud and d is the distance between their centres, to within 10^{-4} at all three tested distances (Fig. 8A; See Data S36 in SI). Since the Gaussian clouds are not the shape of electronic matter, the test was repeated for clouds whose matter thins exponentially with increasing distance from the nucleus, as in the case of hydrogen. The results were within 0.1% of Gaussian clouds at six separation distances, including the regions where they overlap and the interaction falls 45% below 1/d (Fig. 8C; See Data S37 in SI). However, when these clouds are treated as sources that deform the medium, the field gives the same strength with the opposite sign. As a result, like clouds attract, as masses do in gravity (Fig. 8B). Conventional physics draws the same line: a vector field (light) makes like charges repel, while scalar and tensor fields make masses attract.

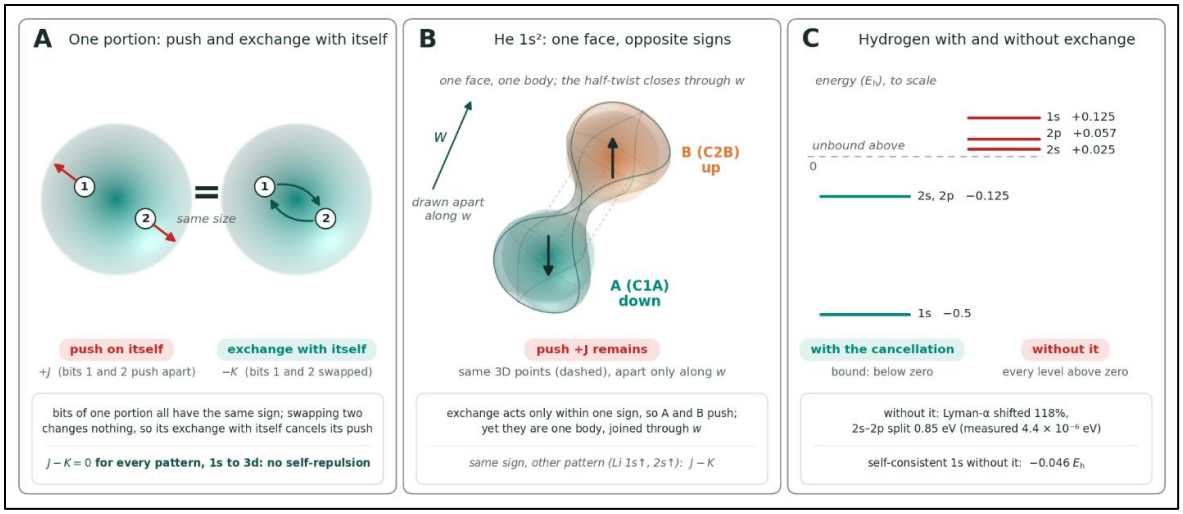

Figure 9. Self-interaction of continuous electronic matter. (A) Interaction within one portion. (B) Interaction between two portions in Helium $1s^2$. (C) Hydrogen levels with and without the cancellation, to scale in E_h.

The second is self-repulsion. Standard QM treats electrons as point particles and omits their self-repulsion by construction. If the electron's charge is spread as real matter, then each part of it should repel the rest. This was one of the objections raised against Schrödinger's charge cloud. In the current model, the portions are not treated as separate objects, but as a continuous body of electronic matter. Thus, applying the exchange rule between a portion and itself, an electrostatic repulsion of a portion on itself and its exchange with itself are then equal and cancel exactly for all six tested patterns from 1s to 3d (Fig. 9A). This is cancellation similar to that in Hartree–Fock theory, where the electron's self-repulsion is removed by its self-exchange. Without it, the hydrogen 1s pattern repels itself by 5/8 E_h. The Lyman-α line then shifts by 118%, the 2s and 2p levels split by 0.85 eV against the measured 4.4×10^{-6} eV, and a self-consistent 1s level rises to –0.046 E_h (Fig. 9C). With it, helium's mean-field energy is −2.861659 E_h, against the Hartree–Fock limit of −2.861680 E_h (See Data S36 in SI).[29] While the continuous electronic matter exchange provides a mechanism for self-exchange, one may ask whether the exchange acts only within one side or crosses over to the other side through the fourth direction, *w* (Fig. 9B).

Table 7. Shift of the hydrogen 1s level for three ways the sign can switch where the body crosses from one side to the other through *w*.

Scenario at the crossing	Fraction of matter of intermediate sign	Shift of the 1s level	Relative shift (ppm)	Consistent with measured lines (≤ 2.9 ppm)
Sharp switch (adopted)	0	0	0	Yes
Gradual switch, spilled fraction	1.3×10^{-5}	0.11 meV	8.3	No
Gradual switch, all matter	1	2.53 eV	1.9×10^{5}	No

To test if the sign switches abruptly or gradually when the continuous body passes from one side to the other through w, three scenarios were compared: a sharp switch at the

crossing; a gradual switch carried by only the spilled fraction of the matter, about 10^{-5}; and a gradual switch carried by all of the matter (Fig. 9B). The results show that the sharp switch aligns with experimental results, whereas the spilled fraction would shift hydrogen's 1s level by 8 ppm, which is beyond the 2.9 ppm agreement of the measured lines, and the fully gradual switch would shift it by 2.5 eV (Table 7; Fig. 9B; See Data S38 in SI).

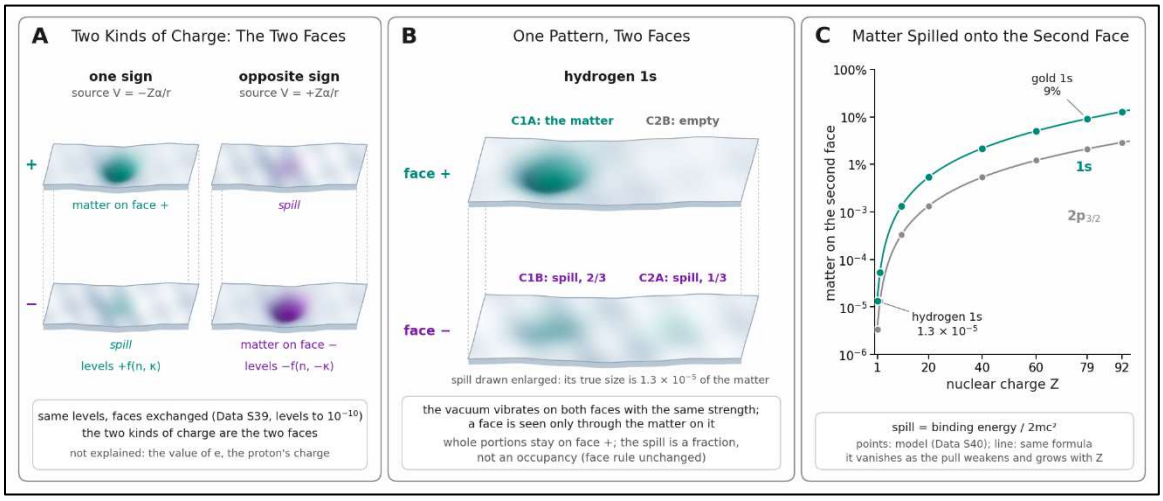

Figure 10. The two faces of the vacuum's vibration. (A) Reversing the sign of the source exchanges the faces: a source of one sign binds matter on face +, the opposite sign on face −, with mirror-image levels. (B) Matter on the second face, equal to the binding energy divided by $2mc^2$, for 1s and $2p_{3/2}$ against nuclear charge Z. Points are model values; lines are the same formula. (C) Hydrogen 1s: the matter sits at C1A on face +. Face − vibrates with the same strength but is seen only through the matter spilled onto it (C1B 2/3, C2A 1/3; drawn enlarged, true size 1.3×10^{-5} of the matter).

The third is why charge comes in two kinds, positive and negative. In VRCM, the field of a positively charged nucleus interacts with two faces of the vacuum's vibration differently. It pulls face+ but pushes on face-. Hence, the electronic matter settles into bound levels only on face+, whereas no matter settles on face-. For hydrogen, the binding energies of all six levels compared (1s, 2s, $2p_{1/2}$, $3p_{1/2}$, $2p_{3/2}$ and $3p_{3/2}$) agree with Dirac's exact formula to 10^{-10}, and the law reproduces Dirac's 2p fine structure of 10.95 GHz for an infinitely heavy nucleus (10,943.7 MHz with hydrogen's reduced mass). When the sign of the source is reversed, the roles are swapped and now face- binds at the levels which are the mirror image of those on face+. The built-in symmetry in the two-face law treats both faces alike; hence the mirroring of levels is exact (Fig. 10A; See Data S39 in SI). Dirac's theory has the same symmetry feature called charge conjugation that gives every electron level a positron partner. Next, the body also has a second two-way feature, the direction of its twist (C1 or C2). However, it plays no part in charge since the two-face law contains no term that depends on it. The two kinds of charge are therefore the two faces of the vacuum's vibration.

$$f = \frac{\int F^2\, dr}{\int (G^2+F^2) dr} \approx \frac{E_b}{2mc^2} \text{ (eq. 12)}$$

where *f* is the fraction of the electronic matter on the empty face, *G* and *F* are the amplitudes on face + and face – (Eq. 10 & 11), E_b is the binding energy, *m* is the mass of the electron and *c* is the speed of light.

Now, in bound mode, the empty face still vibrates with the same strength; however, it is seen only when a small amount of electronic matter is spilled onto it (Fig. 10B). This fraction of matter on the empty face is the binding energy divided by $2mc^2$, which is 1.3×10^{-5} for hydrogen and 9% for the 1s level of gold (Fig. 10C; See Data S40 in SI). In Dirac's theory, this spilled matter is the small component; in VRCM, it is matter on the second face.

Discrete Detection, Interference and the Born Statistics: Why is Continuous Electronic Matter Detected at One Point?

One of the objections to Schrodinger's charge cloud was the detection of electrons as whole at single points rather than as a continuous matter spread like a wave over the whole screen. In QM, the probability of finding an electron at a place is given by $|\psi|^2$ there. In VRCM, the electron is once again treated as a continuous body of matter, so the question becomes how spread matter produces a single dot on the detector, and why the collection of dots ends up as an interference pattern on the screen.

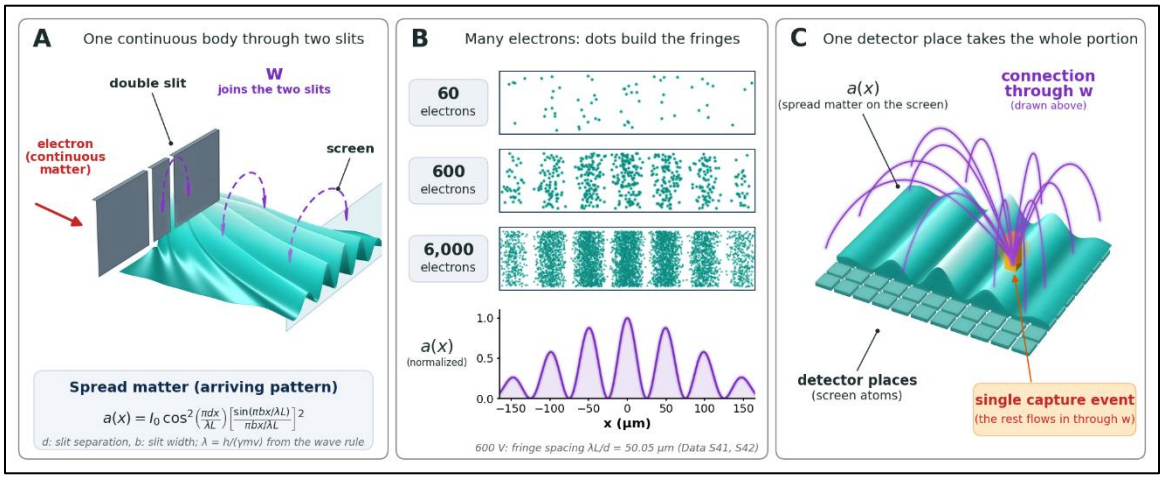

Figure 11. Discrete detection and the build-up of interference fringes. (A) One continuous body passes through both slits, joined through w, and arrives at the screen spread as a(x). (B) Dots from 60, 600 and 6,000 electrons build the fringes of a(x); at 600 V the fringe spacing λL/d is 50.05 μm. (C) The spread matter touches every detector place at once. When one place reaches the detection threshold, the rest of the body flows into it through *w*, giving a single capture event.

To test these questions, the continuous body of electronic matter was spread over 31, 61, 121, and 241 places on the detection screen behind a double slit, following the two-slit pattern, and allowed to evolve (Fig. 11A). For each case, 10,000 runs were performed, and

in every run, the continuous body ended up as a whole at one spot. Additionally, the number of places in which the screen was divided (31 - 241) did not affect the distribution; in every case, each place received the dot as often as its share of the matter, within normal random scatter. Thus, changing resolution didn't change the pattern (χ^2/d_of 0.86 to 1.36; Fig. 11B; Table 8; See Data S41-S43 in SI).

Table 8. Tests of discrete detection, capture odds and apparent size of the electron.

Test	Condition	Result	Criterion/ comparison	Outcome	Data
Capture at a single place	61 places	100% of runs end whole at one place	single dot per electron	Pass	S41
Capture odds vs. matter share	61 places, conserved transfer	χ^2 test: p = 0.619; χ^2/d_of = 1.12	odds = share (Born statistics)	Pass	S41, S42
Dependence on screen resolution	31, 61, 121, 241 places	χ^2/d_of = 0.86–1.36	odds = share at every resolution	Pass	S43
Independent capture (no conservation)	31–241 places	odds ∝ (share)^x x = 3.5—5.2	odds = share	Excluded	S42, S43
Equal-kick rule	3,000 runs	no single dot formed	single dot per electron	Excluded	S41
Largest-share-grows rule	61 places	p = 0	odds = share	Excluded	S41
Apparent electron size	2 eV and 100 GeV probes	2.6 a_o; 2.0 × 10^{-18} m	≤ probe resolution	Pass	S41
Continuous capture	detector-rate capture applied to all matter	2 × 10^7 W mol^{-1} heating	no observed heating	Excluded	S41
Track in a gas	40 ionizations; 10 keV–1 MeV	spread 0.4–0.9 μm between ionizations; path deviation 0.6–2.4 μm	< droplet size (~10 μm)	Pass	S41, S45
Return to earlier shape after capture	as above	path deviation ≈ 1 mm	< droplet size (~10 μm)	Excluded	S41, S45

Physically, when the continuous body of matter leaves the slits and assumes the shape of the vacuum's vibration, some parts have more matter than the others. In the model, the vacuum vibrates in many wavelengths and directions, each shaped by the slits. These vibrations alone show no stripes (visibility 0.000) because vibrations of all wavelengths and directions blur together. Among several vibration patterns, the matter follows only the one whose beat matches its own. That single vibration produces sharp stripes (visibility 0.995) spaced at $\lambda L/d$, where L is the distance from the slits to the screen, and d is the separation of the slits. The wavelength $\lambda = \Gamma/(\gamma mv)$, where γ is the relativistic factor, is obtained from the vacuum's wave rule to within 3 × 10^{-8} at 600 V and 50 kV (See Data S42 and S44 in SI). After exiting the slits, the continuous body is now shaped into thick and thin regions by the existing vacuum vibration, and when it arrives at the screen, it touches the

screen's atoms everywhere at once (Fig. 11C). A constantly vibrating vacuum then randomly moves matter between these atoms, but the total remains one body, so whatever one atom gains, the others lose. The atoms of the screen under the thick region are more likely to fill up first, and once one of them reaches the detection threshold of 99.9%, the rest of the electronic matter flows into it. Atoms under thin regions rarely reach this threshold, and hence the screen appears dimmer in those regions. If each atom on the screen collected matter separately, a place with twice the matter would get the dot 11 to 37 times as often, not twice as often (See Data S42 and S43 in SI). Thus, the correct pattern appears only when matter is treated as a single body.

While the continuous matter can reproduce interference patterns, the electron has always been detected as point-like, and no experiments have measured the size of the electron. In VRCM, the size of the electron depends on the energy of the probe. A 2 eV probe confines the continuous body to 2.6 a_0 (0.14 nm), whereas a 100 GeV probe confines it to 2.0×10^{-18} m. Both of these extremes never appear larger than the resolution of the measurement (0.6 μm for 2 eV and ~2×10^{-18} m for 100 GeV), so every experiment to date finds it point-like. The contraction and expansion of continuous matter happens only during a detection event because, if it happened all the time, at the rate a detector requires, this would heat ordinary matter by 2×10^{7} W per mole (See Data S41 in SI). No such heating is observed, so the matter contracts only when a detection event occurs. Next, a similar process can be envisioned for free electronic matter moving through a gas, as in a cloud chamber. On its path, this matter continuously encounters atoms and ionizes them. In VRCM, each ionization event involves capture of electronic matter that contracts it to about 0.03 nm before it spreads again while moving forward. By the next ionization event, depending on its energy, the matter has grown to only 0.4 – 0.9 μm. In the current study, the simulation of 40 successive ionisation events showed that the ionization points or capture of electronic matter, stayed within 0.6 to 2.4 μm of a straight line, well below the size of a droplet (about 10 μm), and the track appears straight. Had the body returned to its earlier wide shape between the two ionization events, the capture would have been spread over about 1 mm rather than along a straight line (See Data S41 and S45 in SI).

Testable Consequences: Where Does VRCM Depart from QM?

If VRCM reproduces the results of QM wherever both apply, where can it be tested? Since the fourth spatial direction, w, distinguishes VRCM from QM, the testable consequences come primarily from w (Table 9). First, restricting the vibration of the vacuum in *w* creates heavy vibrations that pull slightly harder on electronic matter at the nucleus, lowering only the s-levels. This extra lowering mimics a slightly smaller nucleus and is the same for every

element and for the muon, so it is simply counted as part of the nucleus's size, and atomic spectra cannot reveal w (Table 9, item 1). However, high-energy collisions can test it. If these vibrations act on electronic matter in motion as light does (premise), scattering of fast electron–positron beams at LEP limits w to below 2.6×10^{-19} m (Table 9, item 2; See Data S6 in SI). They would also strengthen the magnetic moments of the electron and the muon (Table 9, item 3), and their squared energies would rise in equal steps, a string-like signature (Table 9, item 4).[33] Because the energy for capture comes from the arriving electron (premise), matter at rest in an atom is never captured spontaneously. VRCM therefore predicts no spontaneous heat or X-ray emission from ordinary matter, unlike collapse models; a confirmed emission would rule out this premise (Table 9, item 5).

Table 9. Testable consequences of the fourth spatial direction *w*.

	Consequence	Origin in VRCM	Experimental test	Present status
1	s-levels lowered as by a slightly smaller nucleus: r^2 reduced by 2.08 ℓ^2, the same for H, D, He^+ and muonic H	Heavy vibrations of w at the nucleus	Atomic spectroscopy; nuclear radii predicted independently to ~0.1%	Absorbed into the measured nuclear size; not detectable at present
2	Extent of $w \leq 2.6 \times 10^{-19}$ m	Heavy vibrations acting on electronic matter in motion (premise)	High-energy e^+e^- scattering	Bound set by LEP
3	Magnetic moments strengthened in proportion to mass squared; muon/electron ratio 4.3×10^4	Heavy vibrations acting on the circular vibration of the electron	Electron and muon $g-2$	Within present bounds
4	Squared energies of the heavy vibrations rise in equal steps ($m^2 \propto n$); first values 1.5, 2.2 and 2.7 TeV	Restricted vibration across w	Searches for heavy states at future colliders	Beyond present reach
5	No spontaneous heat or X-ray emission from matter at rest	Energy for capture from the arriving electron (premise)	Underground germanium detectors	Consistent with present data; distinguishes VRCM from collapse models

CONCLUSION

VRCM revisits Schrödinger's original continuous electronic matter idea by describing the atom without using conventional wavefunctions, quantum numbers or configuration space. In particular, the electron is envisioned as one continuous stationary body of matter that is vibrating locally within patterns of the vacuum, determined by the nucleus, and extending into a fourth direction no larger than 2.6×10^{-19} m. Its portions occupy places defined by pattern, fold and side, and the two folds of a pattern are mirror images that share one 3D shadow and twist oppositely through the fourth direction.

Much of atomic structure is derived from this geometry with nothing fitted. Because the body is non-orientable, one circuit carries a side onto the opposite side and a second returns it, which derives the 720° return and the half-angle share $\cos^2(\theta/2)$. The same reversal derives the change of sign when two portions are exchanged, which quantum mechanics postulates as the antisymmetry of fermions. The magnetic moment is derived from a degenerate pair of winding ½ and a local circular vibration of matter that does not move. Each place holds one hydrogen-equivalent of matter, and under the face rule, taken as a premise, the two places of a face share one 3D shadow, which gives two portions per pattern and with it the shells and multiplicities of elements from hydrogen to neon. The ordering of lithium's 2s below its 2p is also derived within 3% of the measured gap, with every 2s free of 1s matter, as are the triplet ground state of O_2, helium's single opposite-side arrangement with total spin zero, which makes it purely diamagnetic with a susceptibility within 0.7% of the measured value, and the n^2 families from twist counting. Hund's first two rules are derived from the exchange sign and the half-angle push along the body, giving the correct ground terms from boron to fluorine. Collective vibrations of the body capture most of helium's correlation energy, and a coupling between its portions, fixed on helium alone, brings the correlation energies of the helium-like ions from Li^+ to Ne^{+8} within 0.1%, and of H^- within 1.6%, without refitting.

Other than the standard inputs such as the electron's mass, the speed of light, the electron charge and the nuclear masses, the one-electron spectra of hydrogen-like species are set by a single calibrated quantity, the action unit Γ of the vacuum's vibration. Γ plays the role of Planck's constant in VRCM; one value fits five measured hydrogen transitions within 1.3×10^{-9} and fifteen lines within 2.9 ppm. Nothing else is calibrated. With the coupling between the faces taken as a premise, the two-face law derives $g_s = 2$ with no magnetic moment assigned to the electron. From the vacuum's zero-point vibrations, VRCM derives the 2s–2p Lamb shift and anomalous moment of the electron ($\alpha/2\pi$) within 0.67% and 1.7×10^{-7}, respectively.

The same two-face law also derives the two kinds of charge as the two faces: a source of one sign binds matter only on one face, the opposite source only on the other, at mirrored levels that match Dirac's hydrogen levels to ten significant digits. A small fraction of the continuous body, about $\alpha^2/4$ for hydrogen, spills onto the second face. This spilled matter is the small component of Dirac's equation. This law has Dirac's form, and VRCM provides a physical picture of his abstract large and small components as the matter on the two faces of one continuous body. Between two charges, the sign of the force depends on how the field is interpreted: like charges repel only when it is a shift in the timing of the vibration, and would attract if it were a deformation of the vacuum. For all patterns from 1s to 3d, a portion within a fold does not repel itself because the self-repulsion is exactly cancelled by

exchange. Further, the exchange does not cross over w, hence, the portions on opposite sides repel with full strength. Any crossing over *w* requires a sharp switch in sign because a gradual switch shifts hydrogen's lines beyond what is measured.

The same continuous body also accounts for the point-like detection of electronic matter through the mechanism of contraction and expansion. Between captures, this body spreads as a wave of wavelength $h/(\gamma mv)$, derived from the vacuum's wave rule. The Born rule, a postulate in QM, follows from the body remaining whole as it contracts onto one place upon capture. Since the contracted body lies below any probe's resolution, it appears point-like. Since this contracted body only slightly expands before the next capture, successive captures in a gas chamber form a straight line. The geometry with the fourth direction w also bears on quantum entanglement. The VRCM gives Bell correlations without signalling when two portions of one body connected through w, with connection through w taken as a premise, are separated. A full treatment lies outside the scope of this paper and will be presented separately.

VRCM gives one physical picture of the electron's spin and magnetic moment, Pauli exclusion and the Born rule, which quantum mechanics takes as postulates, and of Hund's rules and quantum entanglement: continuous matter at rest in the vibrating vacuum, connected through a fourth spatial direction.

Corresponding Author Contact:

dvidhani@mdc.edu

Data Availability Statement

The original contributions presented in this study are included in the article. All reported results and values can be fully reproduced using the codes developed for this work. The data and codes are available upon reasonable request from the corresponding author at dvidhani@mdc.edu. Further inquiries may also be directed to the corresponding author.

Funding Statement

This work was completed without external grant support or dedicated internal research funding from the participating institutions.

Acknowledgements

D.V.V. gratefully acknowledges Dr. Helen Muniz, Dean of Faculty at Miami Dade College, for her strong encouragement of the continued pursuit of this research and for providing sustained institutional support. The author also extends sincere thanks to Dr. Ramos Felix, Chair of the Department of Mathematics and Natural Sciences at Miami Dade College, for his steadfast support and encouragement. D.V.V. also acknowledges Ms. Sudha for valuable discussions. D.V.V is especially grateful to Dr. Manoharan Mariappan for critically reviewing the manuscript, providing insightful comments, and evaluating the soundness of the computational methodology used in this work.

Conflicts of Interest

The author declares no conflicts of interest.

TOC Graphic

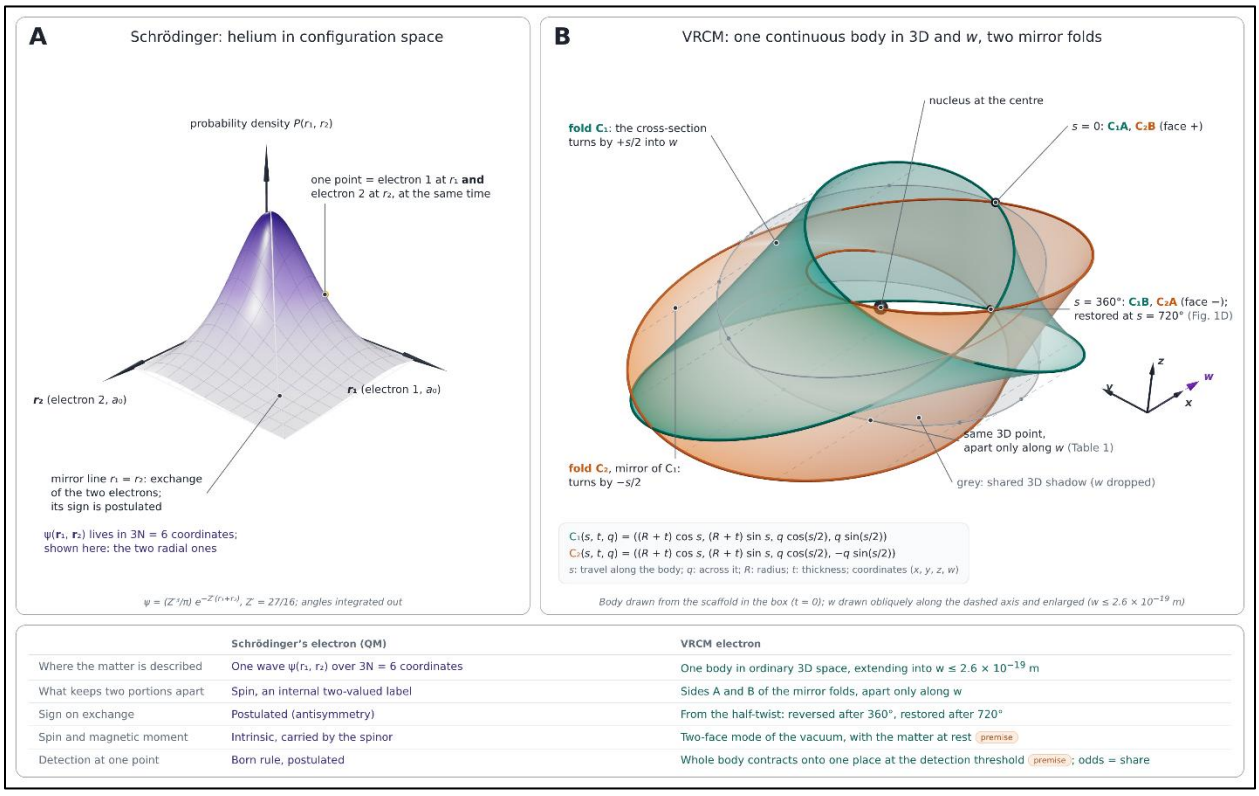

	Schrödinger's electron (QM)	VRCM electron
Where the matter is described	One wave ψ(r₁, r₂) over 3N = 6 coordinates	One body in ordinary 3D space, extending into w ≤ 2.6 × 10^{-19} m
What keeps two portions apart	Spin, an internal two-valued label	Sides A and B of the mirror folds, apart only along w
Sign on exchange	Postulated (antisymmetry)	From the half-twist: reversed after 360°, restored after 720°
Spin and magnetic moment	Intrinsic, carried by the spinor	Two-face mode of the vacuum, with the matter at rest premise
Detection at one point	Born rule, postulated	Whole body contracts onto one place at the detection threshold premise; odds = share

References

[1] Schrödinger, E. An undulatory theory of the mechanics of atoms and molecules. *Phys. Rev.* **28**, 1049–1070 (1926). DOI: https://doi.org/10.1103/PhysRev.28.1049

[2] Gao, S. Is an Electron a Charge Cloud? A Reexamination of Schrödinger's Charge Density Hypothesis. *Found Sci* **23**, 145–157 (2018). https://doi.org/10.1007/s10699-017-9521-3

[3] Monton, B. Wave Function Ontology. *Synthese* **130**, 265–277 (2002). https://doi.org/10.1023/A:1014493527177

[4] Born, M. Quantenmechanik der Stoßvorgänge. *Z. Physik* **38**, 803–827 (1926). https://doi.org/10.1007/BF01397184

[5] Lorentz, H.A. (1937). Electromagnetic Phenomena in a System Moving with any Velocity Smaller than that of Light. In: Collected Papers. Springer, Dordrecht. https://doi.org/10.1007/978-94-015-3445-1_5

[6] Van Vleck, J. H. The Theory of Electric and Magnetic Susceptibilities (Oxford University Press, 1932).

[7] van Leeuwen, H.-J. Problems in the electronic theory of magnetism. *J. Phys. Radium* **2**, 361–377 (1921). https://doi.org/10.1051/jphysrad:01921002012036100

[8] Ohanian, H. C. What is spin? *Am. J. Phys*. **54**, 500–505 (1986). https://doi.org/10.1119/1.14580

[9] Pauli, W. Zur Quantenmechanik des magnetischen Elektrons. *Z. Physik* **43**, 601–623 (1927). https://doi.org/10.1007/BF01397326

[10] Lorentz, H. A. Electromagnetic phenomena in a system moving with any velocity smaller than that of light. *Proc Acad. Sci. Amsterdam* **6**, 809–831 (1904).

[11] Uhlenbeck, G., Goudsmit, S. Spinning Electrons and the Structure of Spectra. *Nature* **117**, 264–265 (1926). https://doi.org/10.1038/117264a0.

[12] Dirac, P. A. M. The quantum theory of the electron. *Proc. R. Soc. Lond. A* **117**, 610–624 (1928) *ibid*. **118**, 351–361 (1928). https://doi.org/10.1098/rspa.1928.0023

[13] Madelung, E. Quantentheorie in hydrodynamischer Form. *Z. Physik* **40**, 322–326 (1927). https://doi.org/10.1007/BF01400372

[14] Wallstrom, T. C. Inequivalence between the Schrödinger equation and the Madelung hydrodynamic equations. *Phys. Rev. A* **49**, 1613–1617 (1994). https://doi.org/10.1103/PhysRevA.49.1613

[15] De Broglie, L. La mécanique ondulatoire et la structure atomique de la matière et du rayonnement. *J. Phys. Radium* **8**, 225–241 (1927).

[16] Bohm, D. A suggested interpretation of the quantum theory in terms of "hidden" variables. I. *Phys. Rev.* **85**, 166 (1952).

[17] Jaynes, E. T. & Cummings, F. W. Comparison of Quantum and Semiclassical Radiation Theories with Application to the Beam Maser. *Proc. IEEE* **51**, 89–109 (1963). https://doi.org/10.1109/PROC.1963.1664

[18] Barut, A. O. & Dowling, J. P. Self-Field Quantum Electrodynamics: The Two-Level Atom. *Phys. Rev. A* **41**, 2284–2294 (1990). https://doi.org/10.1103/PhysRevA.41.2284

[19] Ghirardi, G.C., Grassi, R. & Benatti, F. Describing the macroscopic world: Closing the circle within the dynamical reduction program. *Found Phys* **25**, 5–38 (1995). https://doi.org/10.1007/BF02054655

[20] Allori, V., Goldstein, S., Tumulka, R. & Zanghi, N. On the Common Structure of Bohmian Mechanics and the Ghirardi-Rimini-Weber Theory. *arXiv quant-ph/0603027* (2006). https://doi.org/10.48550/arXiv.quant-ph/0603027

[21] Egg, M. & Esfeld, M. Primitive ontology and quantum state in the GRW matter density theory. *arXiv quant-ph* 1410.8652 (2014). https://doi.org/10.48550/arXiv.1410.8652

[22] Bassi, A. & Ghirardi, G. C. Dynamical Reduction Models. *Phys. Rep.* **379**, 257–426 (2003). https://doi.org/10.1016/S0370-1573(03)00103-0

[23] Fock, V. On the Theory of the Hydrogen Atom. *Z. Physics* **98**, 145–154 (1935). https://doi.org/10.1007/BF01336904

[24] Uehling, E. A. Polarization Effects in the Positron Theory. *Phys. Rev.* **1935**, *48*, 55–63. https://doi.org/10.1103/PhysRev.48.55

[25] Drake, G. W. F. & Swainson, R. A. Bethe Logarithms for Hydrogen up to n = 20, and Approximations for Two-Electron Atoms. *Phys. Rev. A* **41**, 1243–1246 (1990). https://doi.org/10.1103/PhysRevA.41.1243

[26] Bohm, D. & Pines, D. A Collective Description of Electron Interactions: III. Coulomb Interactions in a Degenerate Electron Gas. *Phys. Rev.* **92**, 609–625 (1953). https://doi.org/10.1103/PhysRev.92.609
[27] Pekeris, C. L. 1^1S and 2^3S States of Helium. *Phys. Rev.* **115**, 1216–1221 (1959). https://doi.org/10.1103/PhysRev.115.1216
[28] Drake, G. W. F. High Precision Calculations for Helium. In *Springer Handbook of Atomic, Molecular, and Optical Physics*; Drake, G. W. F., Ed.; Springer: New York, 2006. https://doi.org/10.1007/978-0-387-26308-3_11
[29] Clementi, E. & Roetti, C. Roothaan–Hartree–Fock Atomic Wavefunctions. *At. Data Nucl. Data Tables* **14**, 177–478 (1974). https://doi.org/10.1016/S0092-640X(74)80016-1
[30] Slater, J. C. The Theory of Complex Spectra. *Phys. Rev.* **34**, 1293–1322 (1929). https://doi.org/10.1103/PhysRev.34.1293
[31] Condon, E. U. & Shortley, G. H. *The Theory of Atomic Spectra*; Cambridge University Press: Cambridge, 1935.
[32] Boyd, R. J. A Quantum Mechanical Explanation for Hund's Multiplicity Rule. *Nature* **310**, 480–481 (1984). https://doi.org/10.1038/310480a0
[33] Karch, A. & Katz, E.; Son, D. T.; Stephanov, M. A. Linear Confinement and AdS/QCD. *Phys. Rev. D* **74**, 015005 (2006). https://doi.org/10.1103/PhysRevD.74.015005

Supplementary Files

This is a list of supplementary files associated with this preprint. Click to download.

- VRCMSupportingInformation.pdf